University of Glasgow | School of Chemistry

Synthesis of Unnatural Fluorescent α-amino acids

Ben Gourlay – xxxxxxxx

MRes Chemistry

Supervisor: Dr Andrew Sutherland

Abstract

Unnatural α-amino acids are important probes that can be incorporated into proteins and peptides for biological study using fluorescence spectroscopy. The objective of this MSc research programme was to investigate the synthesis of novel fluorescent unnatural amino acid using transition metal catalysis to implement the key steps.

The aim of the first project was to construct a phenoxathiin α-amino acid and to extend its conjugation by halogenation and subsequent Suzuki-Miyaura reactions. Initially, the phenoxathiin α-amino acid core was prepared using a dual catalytic thioarylation reaction using iron triflimide as a Lewis acid and diphenyl selenide as a Lewis base, followed by a copper mediated cyclisation. Various approaches using succinimide and saccharin reagents were investigated for halogenation but due to either poor conversions or difficult separations, an effective halogenation was not possible. However, the reaction with *N*-iodosaccharin did give access to a novel phenoxathiin-sulfoxide α-amino acid which displayed fluorescent properties with an emission maximum at 372 nm.

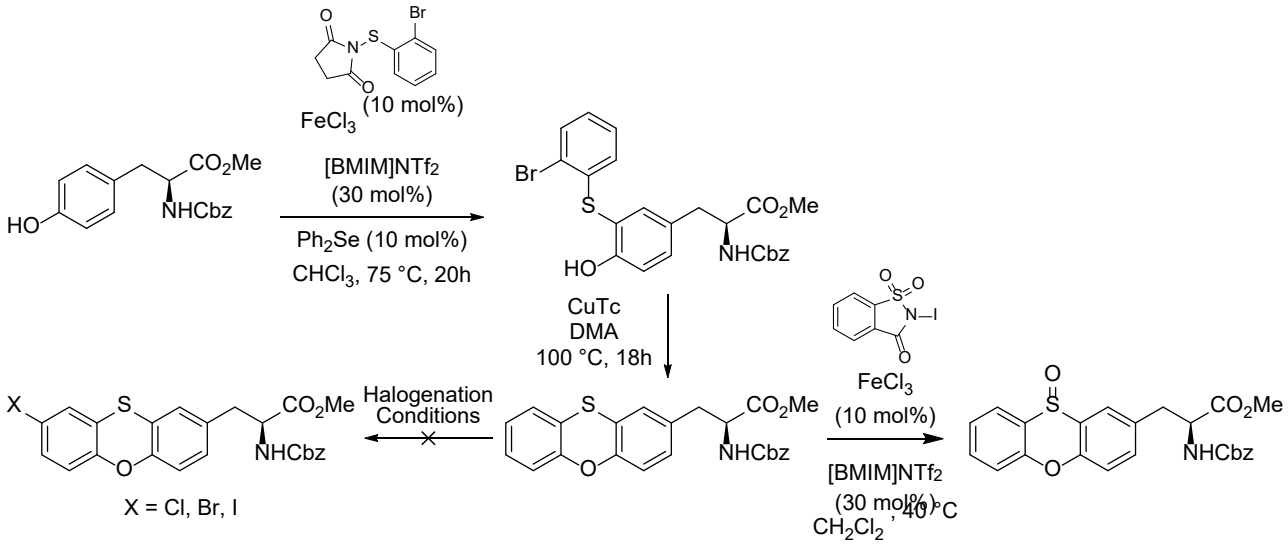

The aim of the second project was to develop a synthesis of a nitro-substituted dibenzofuran α-amino acid. The strategy involved the synthesis of a biaryl analogue of tyrosine, followed by a metal-catalysed C–H activation and cyclisation reaction. Initially, the cyclisation precursor was prepared in three steps. This involved amino-group protection, *ortho*-bromination and then Suzuki-Miyaura cross-coupling reaction with 4-nitrophenyl boronic acid. The first attempted cyclisation used a palladium catalyst and a per-ester as the oxidant was successful but gave the product in only

6% yield. Other methods were investigated in an effort to improve the efficiency of this transformation. Using a simpler method involving a copper(II)-mediated single electron transfer cyclisation was more efficient and gave the desired nitro-substituted dibenzofuran α-amino acid in 16% yield.

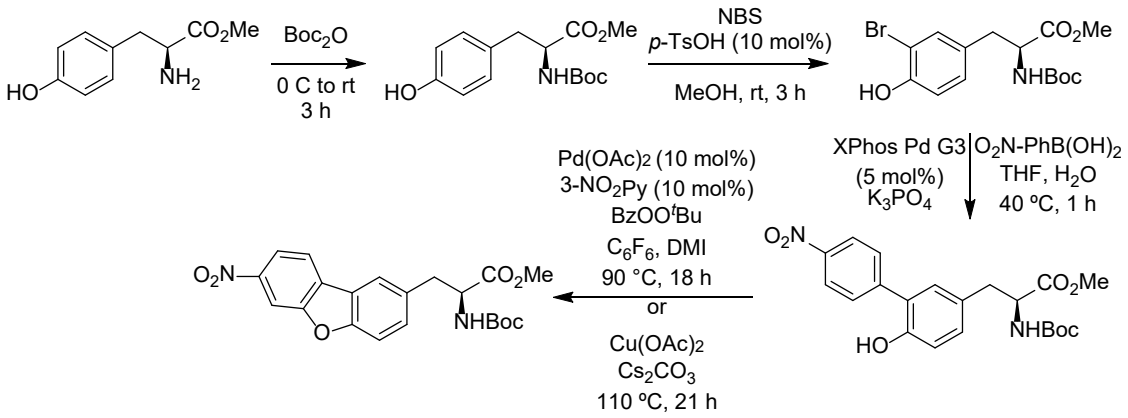

Contents

Abbreviations

°C	Degrees celsius
BINAP	(2,2′-bis(diphenylphosphino)-1,1′-binaphthyl)
[BMIM]NTf_2	1-Butyl-3-methylimidazolium bis(trifluoromethylsulfonyl)imide
BODIPY	4,4-difluoro-4-bora-3a,4a-diaza-s-indacene
$CDCl_3$	Deuterated chloroform
DEPT	Distortionless Enhancement by Polarization Transfer
DIPEA	N,N-Diisopropylethylamine
DMEDA	1,2-Dimethylethylenediamine
DMF	*N,N*-Dimethylformamide
DMSO	Dimethyl sulfoxide
dppf	1,1′-bis(diphenylphosphino)ferrocene
equiv.	Equivalents
FDA	Food and Drug Administration
FMO	Frontier molecular orbital
FRET	Förster resonance energy transfer
g	Gram(s)
GFP	Green fluorescent protein
HOMO	Highest occupied molecular orbital
h	Hour(s)
ICT	Intramolecular charge transfer
IR	Infrared spectroscopy
LUMO	Lowest occupied molecular orbital
M	Molar

mL	Millilitre(s)
mmol	Millimole(s)
mol	Mole(s)
MOM	Methoxymethyl ether
Mp	Melting point
NBS	*N*-Bromosuccinimide
NCS	*N*-Chlorosuccinimide
NMR	Nuclear magnetic resonance
NTf_2	Bis(trifluoromethylsulfonyl)imide
OAc	Acetate
PET	Photoinduced electron transfer
rt	Room temperature
SET	Single electron transfer
SPPS	Solid-phase peptide synthesis
TBAF	Tetra-*n*-butylammonium fluoride
TFA	Trifluoroacetic acid
THF	Tetrahydrofuran
TICT	Twisted intramolecular charge transfer
TLC	Thin Layer Chromatography
UV	Ultraviolet

1.0 Introduction

Fluorescence, a form of luminescence, is a phenomenon that occurs in organic molecules containing π-conjugation. This was originally reported in 1845, by observing the fluorescence of quinine molecules (Figure 1) present in tonic water, but the mechanism of fluorescence was not established until 1852.[1] Fluorescent labelling strategies are important tools in the study of biological processes such as signalling pathways, protein interactions, enzyme activity and cell interactions.[2] The use of fluorescent spectroscopy to monitor these processes has several benefits such as its low cost, high spatial resolution and high temporal resolution.[3] This method for biological study has become prevalent since the discovery of the naturally occurring green fluorescent protein (GFP).[4,5] There have also been several examples of labelling biological molecules with fluorophores such as coumarin, rhodamine, BODIPY and fluorescein.[2] The detriment to this strategy is the large size of these existing fluorophores which has been shown to disrupt the biological processes that are being monitored.[6] Due to this problem, there has been a recent drive to develop small-molecule fluorophores which can be integrated into biological molecules without significant disruption to biological structure or activity.

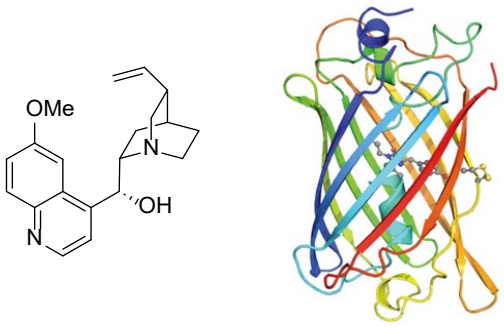

Quinine Green Fluorescent Protein (GFP)

Figure 1: Molecular structure of quinine (left) and protein structure of the green fluorescent protein (GFP) (right).

1.1 Fluorescence

1.1.1 Mechanism of Fluorescence

Fluorescence can occur when the electron of an organic molecule residing in a singlet ground state (S_0) is excited by external stimulus to an excited singlet state (S_1, S_2, *etc.*).[1] The molecule will then rapidly relax to the lowest vibrational energy level of the excited state which is termed internal conversion. As the ground and excited state of the molecules are singlet states, the now excited state is spin-paired with the electron in the ground state. Due to this, the return to the ground state is spin-allowed and, therefore, occurs readily with the emission of a photon. It is also possible for molecules in the excited state to go through intersystem crossing into the triplet state. As the transition to the singlet ground state is now spin forbidden, the relaxation is much slower and this process is called phosphorescence.[7] This phosphorescent pathway is more common in halogenated molecules, as the heavier atoms promote intersystem crossing, as well as when in proximity to paramagnetic species.[8]

This whole process can be represented diagrammatically by a Jablonski plot, named after Alexander Jablonski (Figure 2).[9] In this diagram, the absorption and emission of photons are represented by the straight vertical arrows between the ground and excited states.[7]

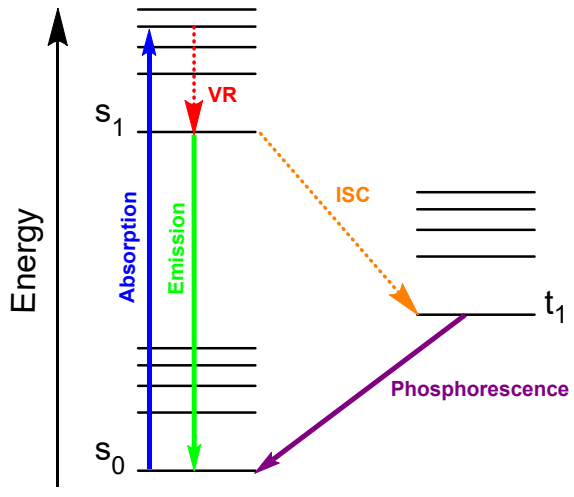

Figure 2: Jablonski diagram with arrows representing absorption, emission, phosphorescence, vibrational relaxation (VR), and inter-system crossing (ISC).

There are various processes which can occur upon excitation of a fluorescent organic molecule. Three significant examples of this are intramolecular charge transfer (ICT), photoinduced electron transfer (PET) and Förster resonance energy transfer (FRET).[10] ICT is often expressed as a push-pull system,[11,12] with fluorophores containing an electron donator and an electron acceptor.[13] ICT occurs in a system where the excited fluorophore possesses a greater dipole moment than the ground state fluorophore. Hence, excitation causes the optimal solvation state to change. This solvent rearrangement is followed by rapid emission of a photon. As the solvent is unable to optimally re-arrange back to match the ground state polarisation, the ground state energy is increased. This leads to a smaller energy gap between the ground and the excited state, causing longer emission wavelengths.[10] PET is another process that can occur upon excitation of a molecule but is often avoided by design when developing organic probes due to it competing with the ICT system. In PET there is a donor electron with an energy between that of the HOMO and LUMO of the fluorophore. The electron is then donated to the orbital which was previously the HOMO before excitation. This causes the pair of electrons to block the relaxation back to the ground state of the molecule.[14] While this mechanism is often avoided in designing highly fluorescent systems it has applications in sensor fluorophore probes which can have activated/deactivated fluorescence based on the initiation of PET in the probe.[15] Finally, FRET is usually an intermolecular process between the excited fluorophore which acts as a donor and another molecule which acts as an acceptor, although this can also occur intramolecularly.[16] This acceptor molecule can be the same compound as the donor, a different fluorophore or a non-fluorescent molecule but must have an energetically compatible excited state vibrational level.[17] In this process, the donor fluorophore transfers the excited state energy to the acceptor molecule causing the excitation of the acceptor molecule. In the case of fluorophore FRET acceptors, this can lead to a subsequent fluorescence emission of the acceptor, or a total lack of fluorescence in the case of the non-fluorescent FRET acceptor.[1]

1.1.2 Fluorescence Parameters

There are various parameters which can be measured and calculated to characterise the photophysical properties of fluorophores for comparison with other fluorescent molecules. An important parameter, particularly for biological applications, is the

absorption maximum and emission maximum.[7] These are derived from the absorption/emission spectra taking the wavelength at the peak intensity for each process (Figure 3). The Stokes shift is then defined as the difference between the absorption and emission wavelength.[7]

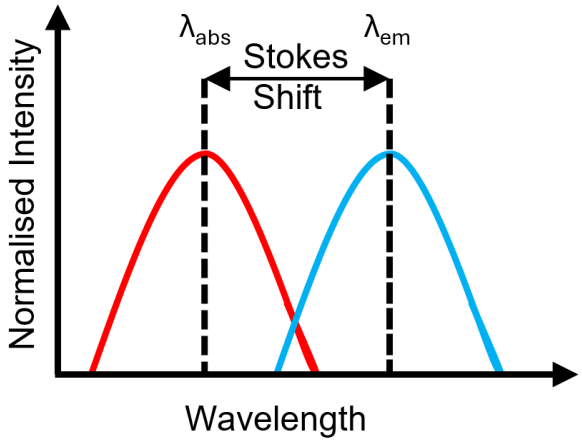

Figure 3: An example fluorescence absorption and emission spectra which defines the absorption (red) and emission (blue) maxima and a visual representation of the Stokes shift.

The quantum yield of a fluorophore is a measure of its efficiency in the fluorescent process. It can be calculated from the ratio of emitted photons and the number of photons that have been absorbed with a maximum possible value of 1.[1] The extinction coefficient is a measurement of the fluorophore's ability to absorb light and is specific to the wavelength of light being absorbed.[7] Finally, the brightness of a fluorophore is one of the most useful metrics for comparison with other molecules. The brightness of a fluorophore is determined by the multiplication of its extinction coefficient and its quantum yield.[8] As this combines the efficiency of the excitation and that of the emission, it gives an overall measure of the entire fluorescent process. A molecule with high brightness allows for a lower detection limit by improving the signal to noise ratio.[8]

1.1.3 Fluorophore Design and Tuning

There is a vast library of small-molecule fluorophores that have been developed for biological applications, the majority of which are based on relatively few fundamental scaffolds.[2,18] Database analysis of the literature in 2020, the six most common principal structures were fluorescein, rhodamine, cyanine, xanthone, coumarin and

BODIPY in decreasing order of popularity (Figure 4).[19] The design of new fluorophores for use in biological systems, both in *vitro* and in *vivo*, needs to be tuned to give suitable properties, particularly with respect to the photophysical parameters previously defined. This is to allow competition with the highly established fluorophores. As the detection of these fluorophores is a major goal, high brightness is important to allow for the precise monitoring of the biological process.[8] This brightness can be achieved by maximisation of the quantum yield, as well as improved extinction coefficients. It is also useful for absorption and emission wavelengths of the fluorophores to be towards the red end of the spectrum. As shorter wavelength light can be damaging to the cells of the biological systems being studied the red-shifted fluorophores are more suited.[20] Additionally, longer wavelengths of light are both absorbed and scattered less by tissues. As such red-shifted fluorophores also allow for greater tissue penetration for imaging purposes.[21] Another important factor is the stability of the fluorescent tag. This stability means both chemical stability against reactive oxygen species found in biological systems,[22] as well as its photostability.[23] The photostability can be improved by tuning the structure to reduce triplet-state lifetimes. In addition to these factors, it remains key that the fluorescent tags are not too large so as not to perturb the systems being studied as larger fluorescent tags are known to interfere with various factors such as protein structure and function[24].

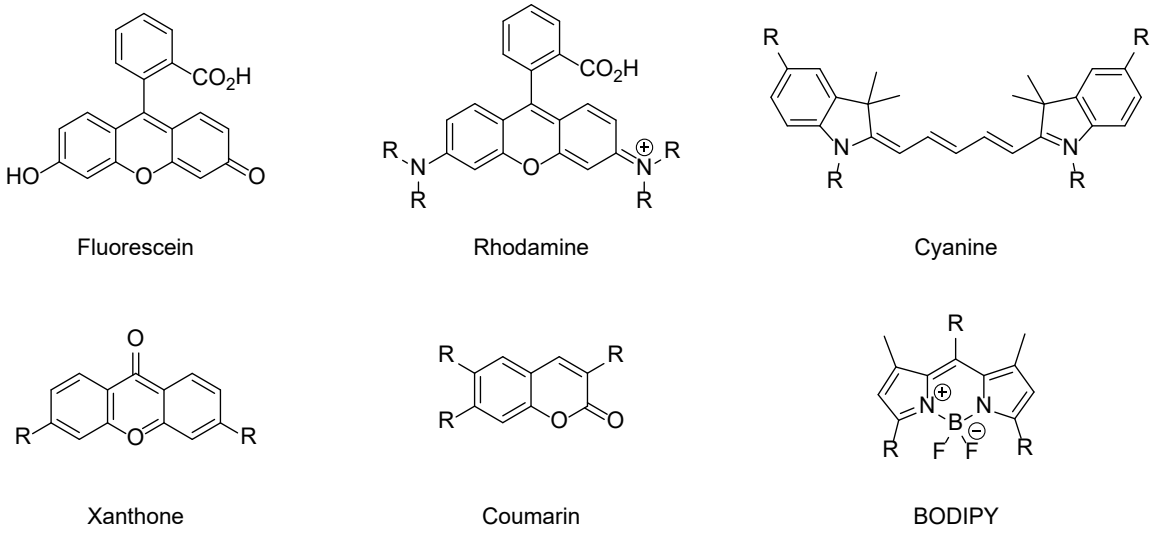

Figure 4: Common fluorophore scaffolds; Fluorescein, rhodamine, cyanine, xanthone coumarin and BODIPY

One strategy in the design of fluorophores is the introduction of electron-donating and electron-withdrawing groups within the molecule. This approach utilises the stabilisation effect that electron-withdrawing groups have on the HOMO and LUMO of the molecule and the destabilising effect brought about by electron-donating groups on the HOMO and LUMO.[25] This can then be combined with frontier molecular orbital theory to reduce the energy gap between the HOMO and LUMO and therefore, selectively red-shift the absorption and emission wavelengths of the fluorophore.[26] For example, the introduction of an electron-withdrawing substituent at a site on the molecule where the LUMO is present and the HOMO is either less localised or not at all represented, will lower the LUMO while not significantly or at all affecting the HOMO. This will give red-shifted fluorescence due to a decrease in energy required to bridge the gap between the molecular orbitals.[26] The same effect can occur from the introduction of an electron-donating substituent at a site with high HOMO density and low or zero LUMO density. This will instead increase the HOMO energy but with the same effect of decreasing the FMO energy gap, providing a red-shifted absorption and emission.

Another method for red-shifting absorption and emission wavelengths of a fluorophore is by extending the conjugation of the π-system.[27] This is explained by the linear combination of atomic orbitals,[28] and is shown below in the example of ethene, butadiene and hexatriene (Figure 5). As the conjugation of the molecules increases there is less significant bonding character of the HOMO and hence an increase in the energy. Similarly, as the conjugation increases there is less anti-bonding character in the LUMOs of the molecules, giving lower energy molecular orbitals. Combined, this will result in a lower energy gap between the FMOs and hence a greater absorption and emission wavelength, red-shifting the fluorophore.

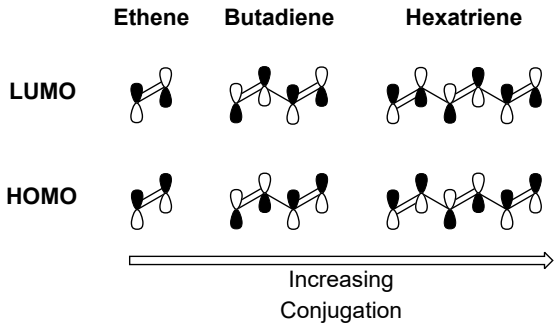

Figure 5: A representation of the linear combination of atomic orbitals (LCAO) for the frontier molecular orbitals of ethene, butadiene and hexatriene.

As well as red-shifting the absorption and emission properties, it is optimal to design fluorophores that have high quantum yields as these will be directly proportional to the molecular brightness. One way this can be achieved is by creating more rigid scaffolds in the fluorophore to minimise bond rotation as flexibility can cause non-radiative energy loss before emission occurs.[8] An example of this can be seen in the example of the replacement of dimethyl amino-substituted coumarin and rhodamine scaffolds with azetidinyl substituents (Figure 6).[29] This shows a significant increase in the quantum yield, owing to the constraint of the bond rotation in the newly-substituted fluorophores. In the case of the diethylamino-substituted coumarin, the replacement with an azetidinyl group causes the quantum yield to be 28 times greater than the original fluorophore.

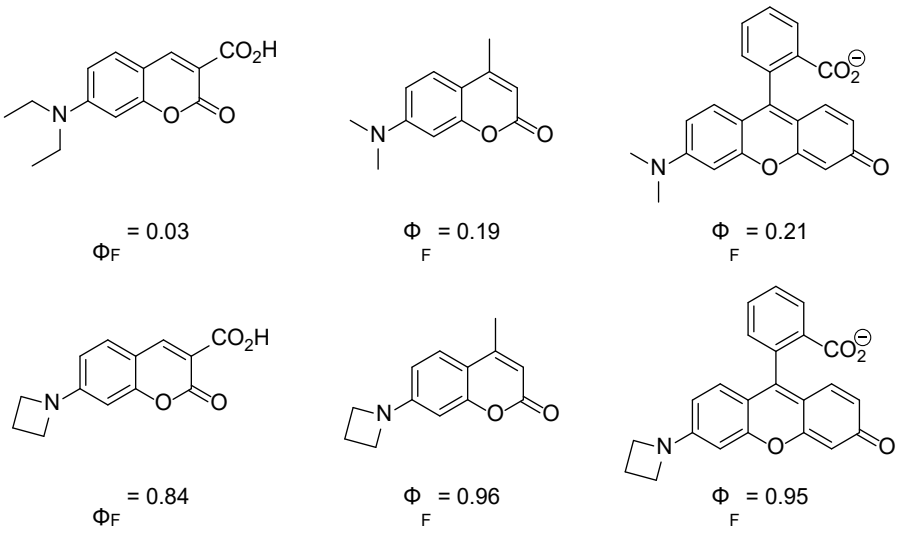

Figure 6: Examples of the quantum yields of fluorophores containing alkyl-substituted amines (top) compared with similar fluorophores with an azetidinyl group (bottom).

1.2 Fluorescent α-Amino Acids

There are three naturally occurring α-amino acids, tryptophan, tyrosine, and phenylalanine, which possess fluorescent properties owing to side-chains with conjugation (Figure 7).[30] These have previously been utilised for the fluorescence detection of proteins for biological study where they are naturally abundant in applications such as the study of the change of protein structure and size.[31] However, this approach has significant limitations due to the restricted number of proteins with a high abundance of these α-amino acid and the weak fluorescent properties of these α-amino acid.[18]

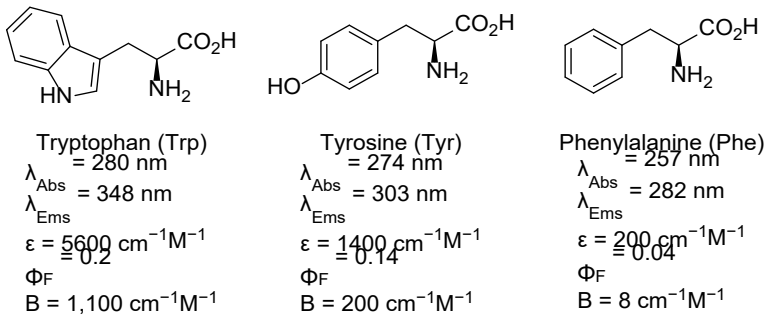

Figure 7: Natural fluorescent α-amino acid tryptophan, tyrosine and phenylalanine and their photophysical properties.

1.2.1 Enhancing α-Amino Acid Fluorescence

Efforts have been made to improve the fluorescent capabilities of α-amino acid by developing new analogues based on natural α-amino acids. Various analogues based on tryptophan have been developed that have improved properties (Figure 8). The aza-tryptophan **1** has a larger Stokes shift and red-shifted absorption and emission wavelengths.[32] 4-Cyanotryptophan **2** has a high quantum yield (Φ_F = 0.8–0.9) and red-shifted absorption and emission wavelengths (λ_{abs} = 325, λ_{em} = 420 nm).[33] This was synthesised using a palladium-catalysed cyanation as the key step. A 4-formyltryptophan fluorophore **3** was also prepared with the position of the formyl group positioned to generate a push-pull fluorophore with the indole nitrogen atom.[34] A study surveying substitution at the 4-position of tryptophans has illustrated the trend of stronger electron-withdrawing groups increasing the absorption and emission wavelengths with the electron-donating groups causing the opposite effect.[35]

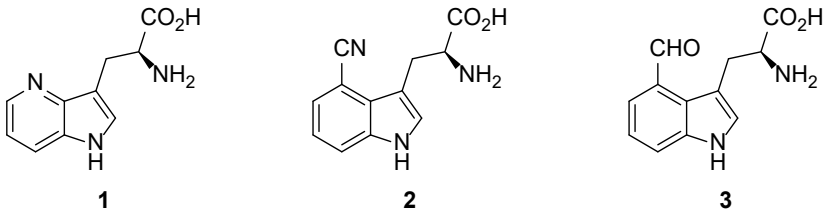

Figure 8: Examples of modified tryptophan analogues and their enhanced photophysical properties.

1.2.2 Modification of α-amino acids

Another strategy for the development of unnatural fluorescent α-amino acid is by incorporating known fluorophores. There have been several examples, utilising a range of synthetic methods. One example is the attachment of BODIPY to the side-chain of tryptophan (Scheme 1).[36] This was achieved using a Pd-catalysed C–H activation reaction of the Fmoc-protected tryptophan derivative **4** and iodo-substituted BODIPY as the key step. The resulting BODIPY coupled α-amino acid (Tryp-BODIPY) **5** was then used for the imaging of fungal infections *in vivo*, acting as a tryptophan surrogate. Further applications included incorporation into multiple peptide sequences such as Apo-15 for *in vivo* labelling of apoptotic cells.[37]

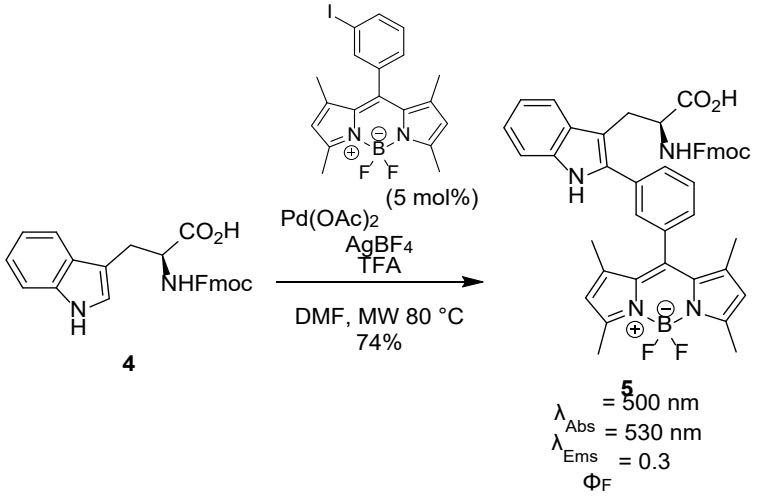

Scheme 1: Pd-catalysed C-H activation to synthesise Tryp-BODIPY

Another synthetic method to access fluorogenic α-amino acid is the use of conjugate addition reactions to create cysteine derivatives with fluorophores linked via the sulfur atom such as in the coumarin-substituted cysteine **8** (Scheme 2).[38] This involves the

1,4-conjugate addition of coumarin-derived thiols with **6,** a chiral bicyclic dehydroalanine motif. The adduct **7** was then hydrolysed under acidic conditions to give **8,** the coumarin-linked cysteine. Incorporation into peptides, such as VPALK and VPALR was then achieved, demonstrating the utility of these fluorescent α-amino acids for biological fluorescent imaging applications.

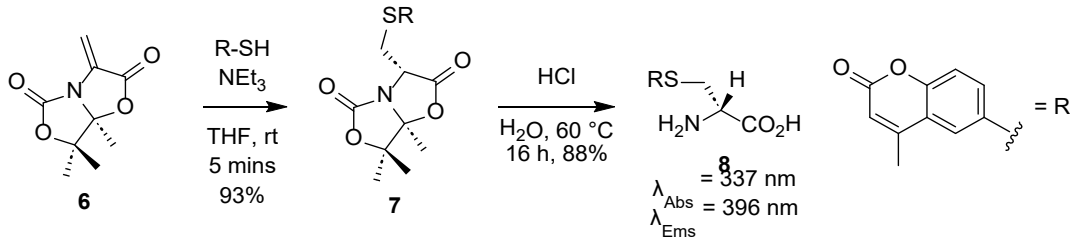

Scheme 2: Conjugate addition as the key step for the synthesis of a coumarin linked cysteine derivative

A further method which is prevalent in unnatural α-amino acid synthesis is using Pd-catalysed coupling reactions to attach fluorophores to the α-amino acid scaffold. An example of this is the synthesis of the biphenyl-substituted phenylalanine derivative **11** (Scheme 3). In this approach, a Suzuki-Miyaura reaction is used for the coupling of 4-biphenyl boronic acid with a *p*-iodophenylalanine derivative **10**.[39,40] Pd-catalysed coupling reactions have proved very useful for extending the conjugation of fluorophores and generating novel unnatural α-amino acid with improved fluorescent properties.[3]

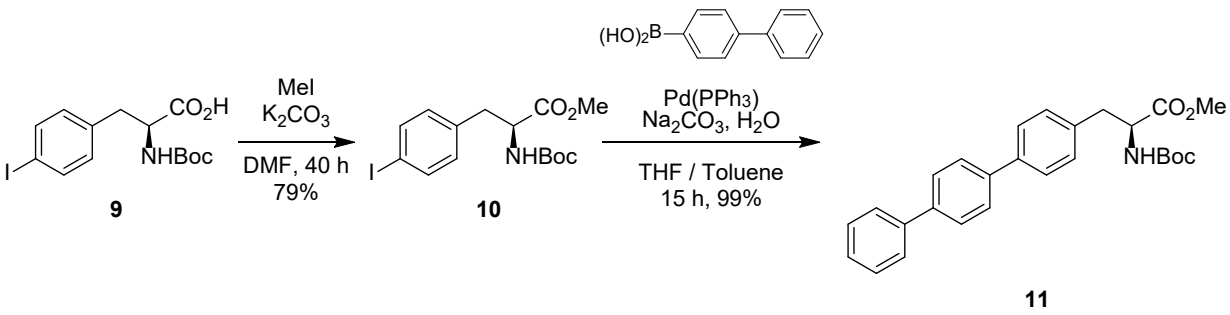

Scheme 3: Synthetic route to biphenyl-substituted phenylalanine derivative

Another palladium-catalysed coupling approach was used for the preparation of acridon-2-ylalanine **14**, which utilises a Buchwald-Hartwig reaction as the key step.[41] The synthetic route started from L-tyrosine, which is protected in three steps in good yield (Scheme 4). The protected L-tyrosine **12** was then reacted with methyl 2-aminobenzoate in the key Buchwald-Hartwig step. The resulting product **13** was then heated in sulfuric acid to initiate a Friedel-Crafts cyclisation and produce the xanthone α-amino acid **14**. This route improved the previous route to **14** that began from *p*-nitrophenylalanine.[42] Photophysical study of **14** shows that it possesses a very high quantum yield (Φ_F = 0.95), giving a bright blue-emitting fluorophore despite a fairly low extinction coefficient[41]. **14** has been incorporated into several peptides and used to monitor peptide binding and protein folding, showing its biological application.

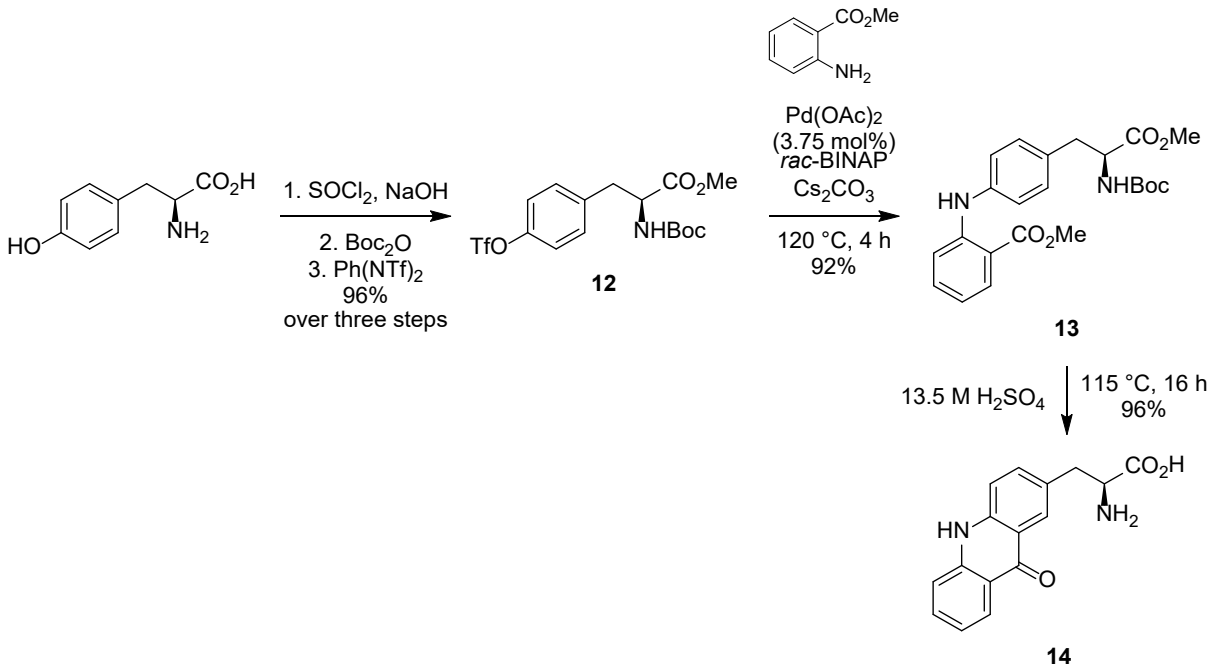

Scheme 4: Synthetic route to acridon-2-ylalanine from L-tyrosine.

Copper-catalysed Ullmann-type reactions have also been used to incorporate a fluorophore into an α-amino acid (Scheme 5).[43] In this example, the protected L-tyrosine derivative **15** was coupled with fluorophores at the phenol group to give pyrene, diphenyl and *p*-nitrobenzene groups. The pyrene α-amino acid **16** displayed

significantly red-shifted absorption (λ_{abs} = 382 nm) illustrating potential for application in the study of biological systems.

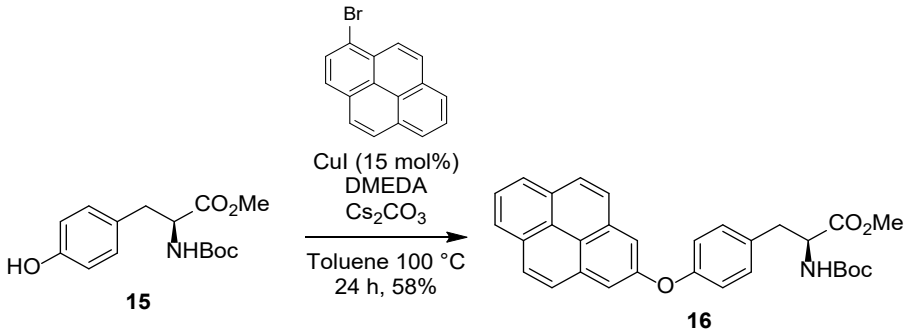

Scheme 5: Synthesis of pyrene-substituted α-amino acid via copper-catalysed Ullman-type reaction

Copper catalysis has also been used for click chemistry for the preparation of fluorescent α-amino acids (Scheme 6).[44,45] In particular, these have been utilised for coupling various alkyne-substituted fluorophores such as **17** to azide α-amino acids to give fluorogenic α-amino acids like **18** with 1,2,3-triazole groups. This was shown to extend the conjugation and give red-shifted absorption and emission wavelengths. Further work building on this has also applied ruthenium catalysis for similar transformations.[46]

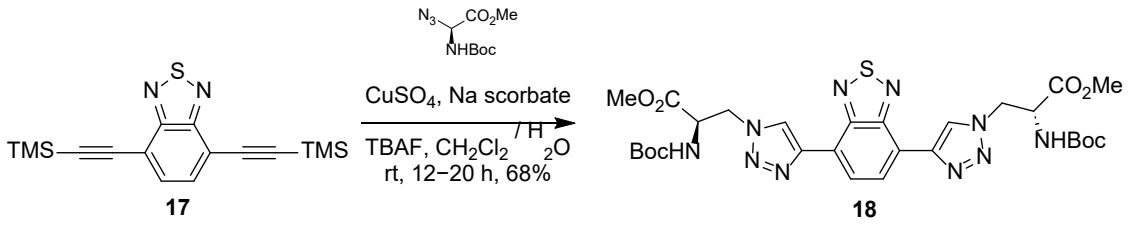

Scheme 6: Copper-catalysed click reaction to synthesise 1,2,3-triazole linked fluorescent α-amino acids

One route by Rück-Braun and co-workers described the synthesis of xanthone α-amino acids with Boc and Fmoc protection.[47] The start of this process involved an optimized copper(I) catalysed coupling reaction between 2-bromo-benzoic acid **19** and 4-methoxyphenol **20** in an Ullmann-like reaction (Scheme 7). Subsequent reaction of **21** with sulfuric acid under reflux mediated the cyclisation to the xanthone scaffold as

well as the hydrolysis of the methoxy substituent forming hydroxyxanthone intermediate **22**. Subsequent treatment of **22** with triflic anhydride and pyridine produced xanthone triflate **23**. Triflate **23** was then subjected to a palladium-catalysed cross-coupling reaction with an orangozinc alanine analogue which is formed in situ, resulting in the final protected xanthone α-amino acids **24**. These unnatural xanthone α-amino acids were used for the study of polypeptide folding using triplet-triplet energy transfer (TTET).

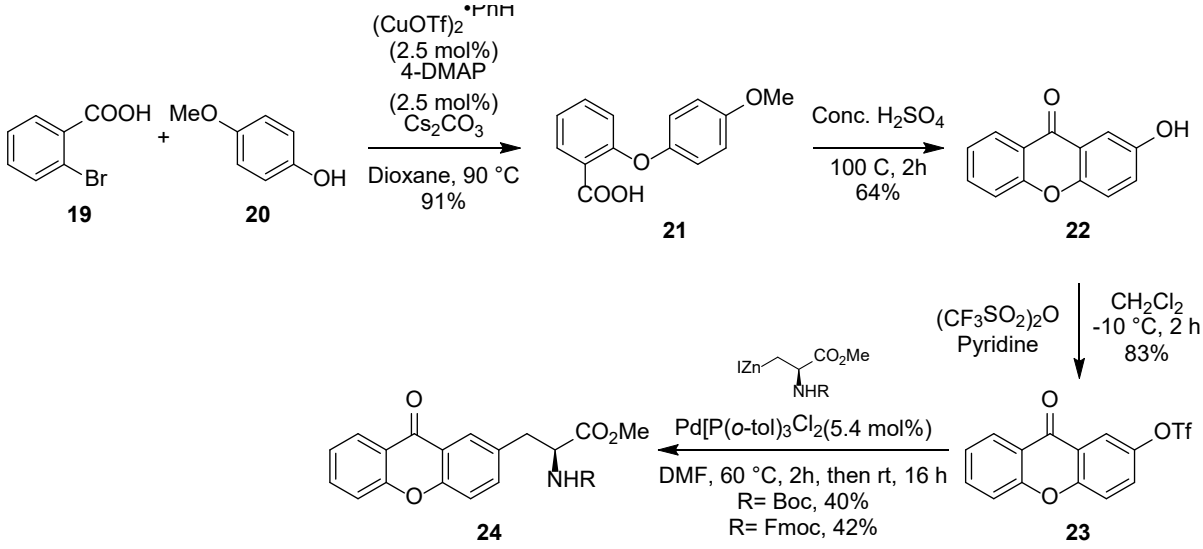

Scheme 7: Synthesis of xanthone α-amino acids via palladium-catalysed coupling

Another example of linking a fluorescent group to α-amino acids is the coupling of coumarins to lysine by formation of a carbamate functional group (Scheme 8).[48] The coumarin was first constructed using a Pechmann condensation reaction between resorcinols and 1,3-acetonedicarboxylate in the presence of an acid giving coumarin starting material **25**. Benzyl protection of phenol **25** under Mitsunobu conditions was then followed by ester hydrolysis to carboxylic acid **26** which was subsequently reduced to alcohol **27** with borane dimethylsulfide. Reaction at this primary alcohol with *N*,*N*′-disuccinimidyl carbonate gave activated coumarin coupling agent **28** in quantitative yield. The key step was then achieved with the reaction between carbonate **28** and the Cbz-protected lysine to form carbamate linked coumarin α-amino acid **29**. A final deprotection yielded the HCl salts of the carbamate linked

coumarin-lysine. These novel unnatural α-amino acids showed fluorescent properties which would be applicable in biological studies using acid conditions.

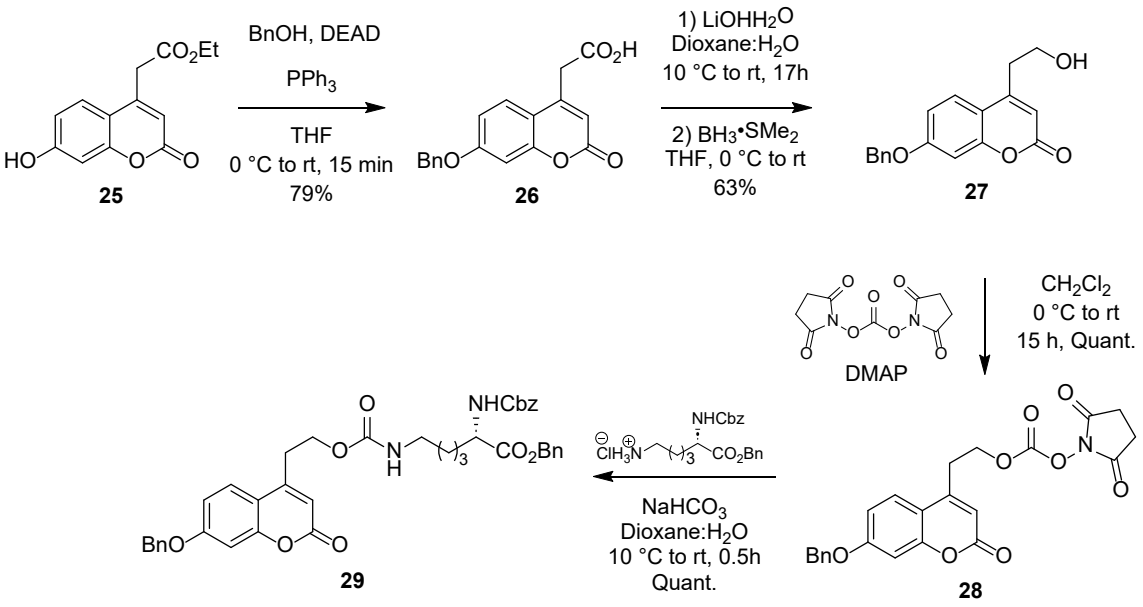

Scheme 8: Synthesis of coumarin substituted α-amino acids via the formation of carbamate linker groups

Incorporation of Fluorescent α-amino acid into Peptides and Proteins

For the application of these fluorescent α-amino acid probes in biological study they first need to be integrated into the biologically relevant species. This is done by solid phase peptide synthesis (SPPS).[3] SPPS is a process where α-amino acids are consecutively coupled with intermittent protection and deprotection while anchored to a solid support. Another method is to genetically encode the unnatural α-amino acid into proteins.[49]

1.2 Previous work in the group

The Sutherland group has previously carried out the development and synthesis of various fluorescent α-amino acids for potential application as biological markers. Early work focused on the synthesis of enone-derived α-amino acids via a Horner-Wadsworth-Emmons (HWE) reaction as the key step.[50] The synthetic route started from L-aspartic acid which was converted to a phosphonate ester **32a** in three steps (Scheme 9). HWE reaction of this with a range of aldehydes allowed the general

preparation of *E*-enones **33** in good yields. This was then applied for the synthesis of a fluorescent α-amino acid **34a** by using 4-dimethylamino-1-naphthaldehyde as the aldehyde for the HWE reaction. This was due to the known fluorescent properties of dimethylaminonaphthalene compounds. The resulting HWE product was produced in 72% yield. The fluorescent properties of the deprotected α-amino acid **35** were then evaluated showing absorption and emission maxima at higher wavelengths than that of naturally occurring α-amino acid. From this, it was suggested that the species **35** had potential as a fluorescent marker to be integrated into proteins and peptides.

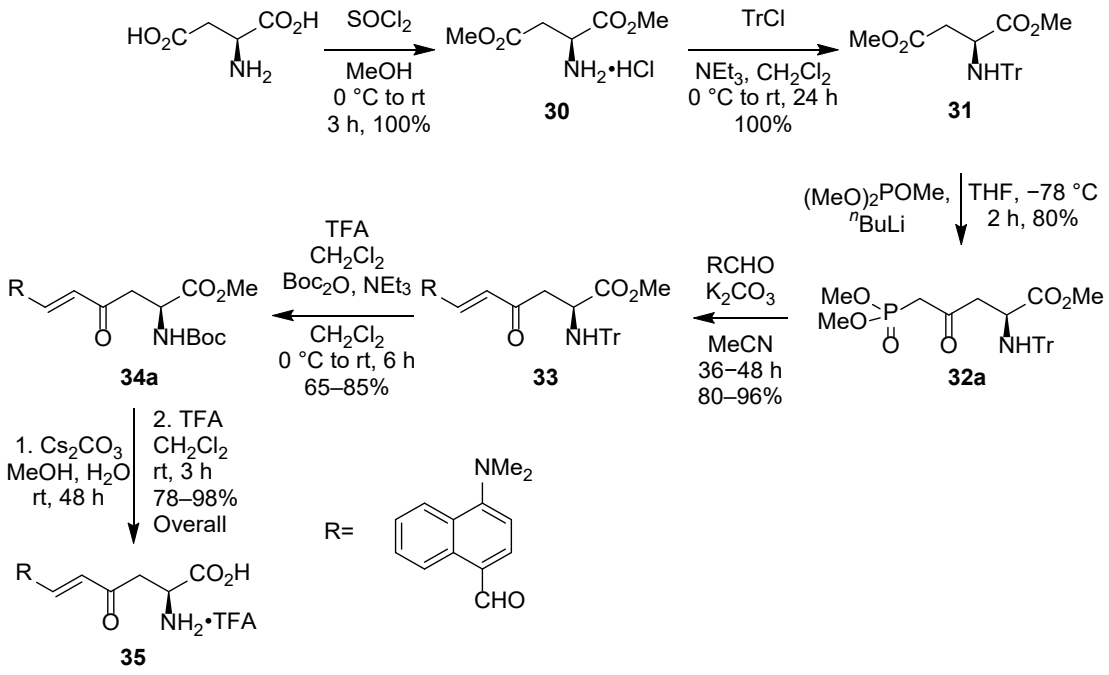

Scheme 9: Synthetic route of enone derivative α-amino acid via a HWE reaction as the key step

This work was then expanded by utilising the enone functionalised α-amino acids in the synthesis of **38**, a fluorescent β-pyridyl α-amino acid with 4-arylpyridyl side chains (Scheme 10).[51] This was achieved by employing the Cbz-protected enone α-amino acid **34b** in ytterbium-catalysed reverse electron-demand hetero-Diels-Alder reactions with ethyl vinyl ether. The resulting dihydropyran was **36** and then transformed into the corresponding pyridine **37** in a modified Knoevenagel-Stobbe reaction using hydroxylamine hydrochloride. Finally, an acid-mediated dual-deprotection of the amine and carboxylic acid gave the β-pyridyl α-amino acid **38**. This design incorporated the push-pull fluorophore design strategy with the electron-deficient pyridine rings

expected to pair well with the electron-rich aryl substituents. This expected trend was observed with the electron-rich-substituted compounds showing strong fluorescence with large Stokes shift and quantum yields. Furthermore, the α-amino acid was shown to be highly sensitive to solvent polarity and was built into a biologically interesting hexapeptide via a Fmoc-based SPPS procedure.

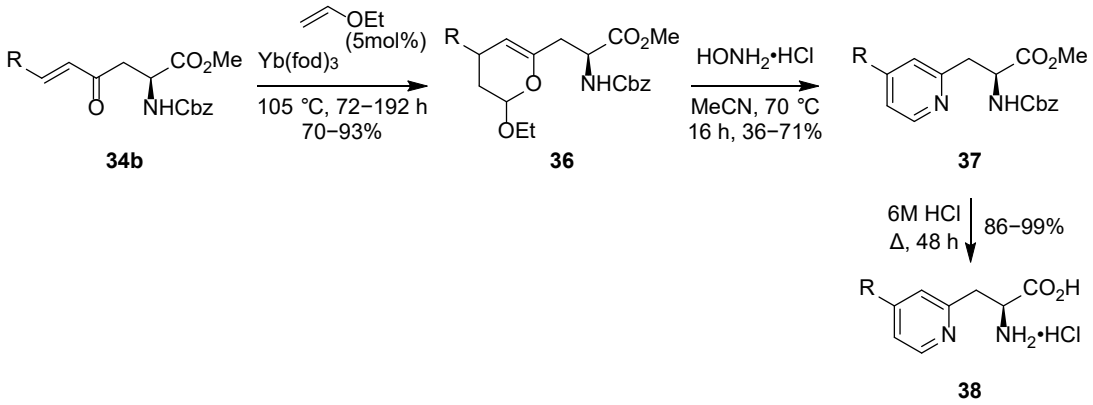

Scheme 10: Synthetic route to fluorescent β-pyridyl α-amino acid with 4-arylpyridyl side chains

To improve quantum yields, α-amino acids with conformationally rigid pyrazoloquinazoline side-chains were developed (Scheme 11).[52] These were synthesised from the previously developed enone derived α-amino acid **32b**. A one-pot condensation and conjugate addition reaction using hydrazine, with a subsequent oxidation was implemented to construct the pyrazole compound **40**. Reduction of the nitro group and reaction with triphosgene in a basic environment allowed for carbonylation and the formation of the pyrazoloquinazoline ring system in **42**. Deprotection then gave the target fluorophore **43**. These α-amino acids proved to be strongly fluorescent, with high quantum yields. The capability of the trimethylamine-substituted variety was displayed by excitation of the fluorophore at 700 nm via two-photon spectroscopy and by incorporation into a biologically relevant peptide using SPPS methodology.

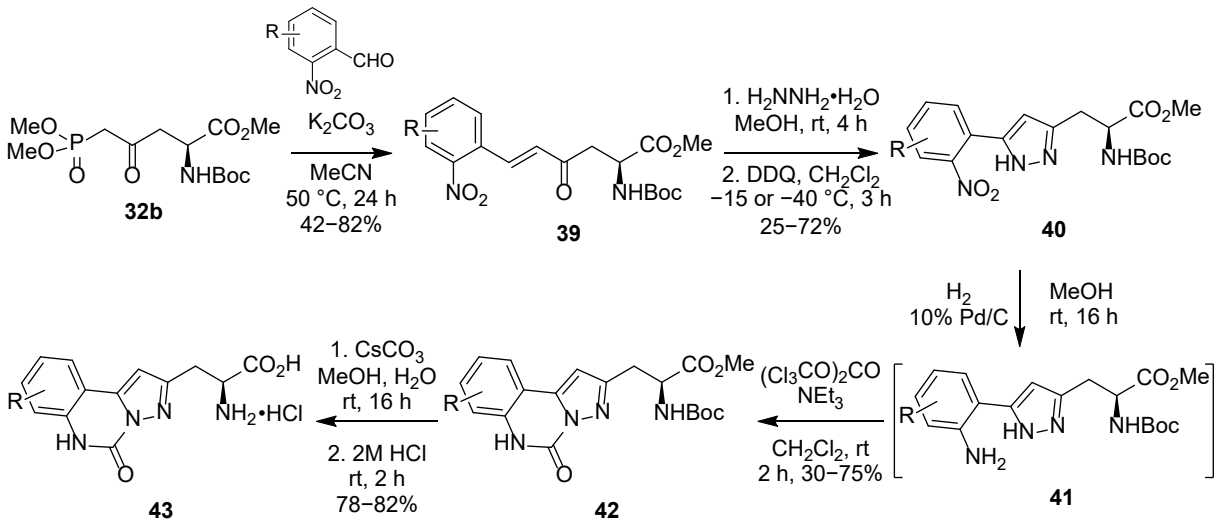

Scheme 11: Synthetic route towards conformationally rigid pyrazoloquinazoline α-amino acid

Other work focused on the synthesis of the benzotriazole-derived α-amino acid **50** (Scheme 12).[53] These were prepared by nucleophilic aromatic substitution of *ortho*-fluoronitrobenzenes with a 3-aminoalanine derivative **46**, followed by reduction of the nitro substituent to the amine **48**. The key step was then cyclisation to the benzotriazole motif containing α-amino acid **49**, using a polymer-supported nitrite reagent in the presence of tosic acid. The scope of these fluorophores was then extended by coupling the bromine-substituted benzotriazole α-amino acid with aryl boronic acids using Suzuki-Miyaura reactions. Henceforth, a study of the photophysical properties of these α-amino acids revealed that the electron-rich aryl-substituted benzotriazole α-amino acid were highly fluorescent in the visible region with MegaStokes shift. The *p*-methoxyphenyl-substituted benzotriazole produced the brightest fluorophore.

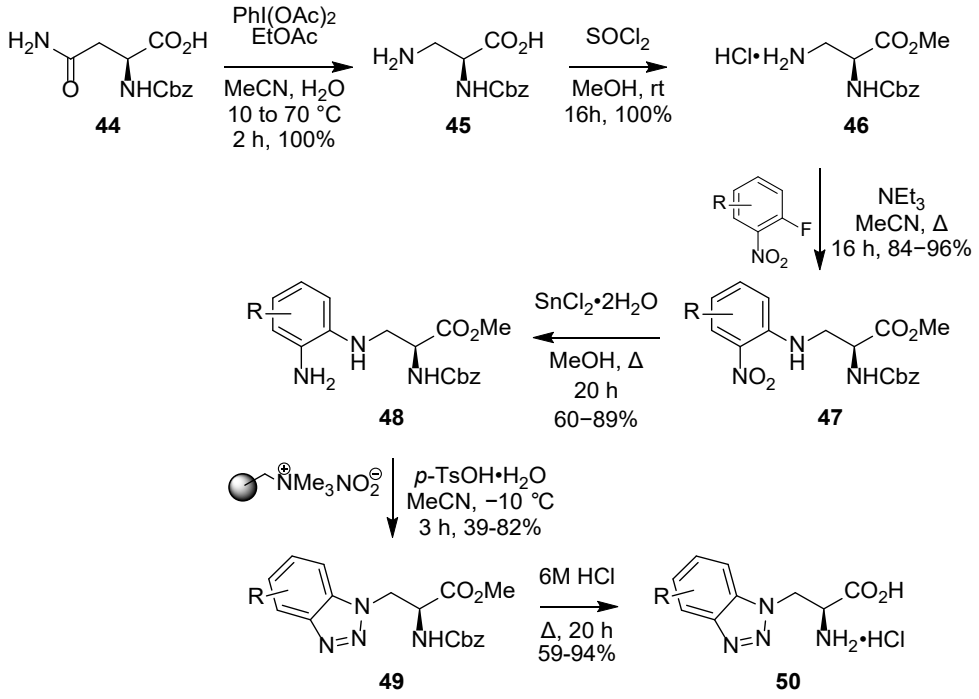

Scheme 12: Synthetic route to a series of benzotriazole-derived α-amino acid

The Sutherland group also developed dual emissive α-amino acids **54** controlled by rotation of bi-aryl systems.[54] These were synthesised by use of the mild diazotisation-heterocyclisation method involving a reaction of a 2-aminobenzamide with a polymer-supported nitrite reagent and *p*-tosic acid to form α-amino acid **52** with a benzotriazinone ring system (Scheme 13). Suzuki-Miyaura reactions were then carried out to substitute arenes at the previously brominated site to provide the further conjugated species **53**. A final deprotection of the compound in two steps yielded the target unnatural α-amino acid **54**. These α-amino acids displayed dual emission fluorescence due to existing in both the locally excited and twisted intramolecular charge transfer (TICT) excited states. Furthermore, alternate electronics and positioning for substitution affected the intensity of the bands. This led to the development of the 2-methoxyphenyl-substituted benzotriazinone, which due to twisting of the biaryl motif, showed bright TICT fluorescence.

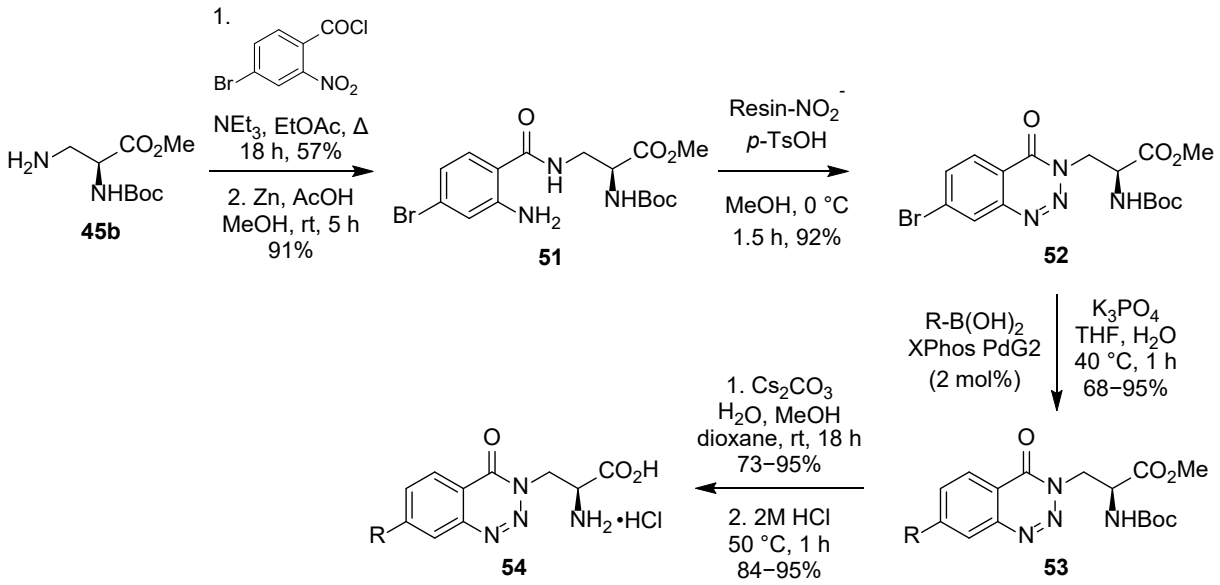

Scheme 13: Synthetic route towards dual emissive α-amino acid controlled by rotation of bi-aryl systems

Further work has produced conjugated benzotriazole derivatives with alkyne **58** and alkene **60** spacers (Scheme 14).[55] The synthetic route started with the nucleophilic aromatic substitution of 2-fluoro-5-iodonitrobenzene with a 3-aminoalanine derivative **45b**, followed by the reduction of the nitro substituent with zinc dust giving the amine **55**. A one-pot process was then utilised to carry out a diazotisation and cyclisation to yield a 5-iodobenzotriazole intermediate **56**. Sonogashira reactions then allowed extension of conjugation by incorporation of alkynes forming the species **57**. It was then possible to access alkenyl-conjugated benzotriazoles **59** via a Pd-catalysed hydrogenation reaction. This method was preferred to Heck and Suzuki-Miyaura coupling to form alkenyl-spaced benzotriazoles as they were low yielding. A photophysical study of the deprotected compounds showed that the alkyne variations **58** possessed higher quantum yields and brightness than previously synthesised biaryl benzotriazoles.

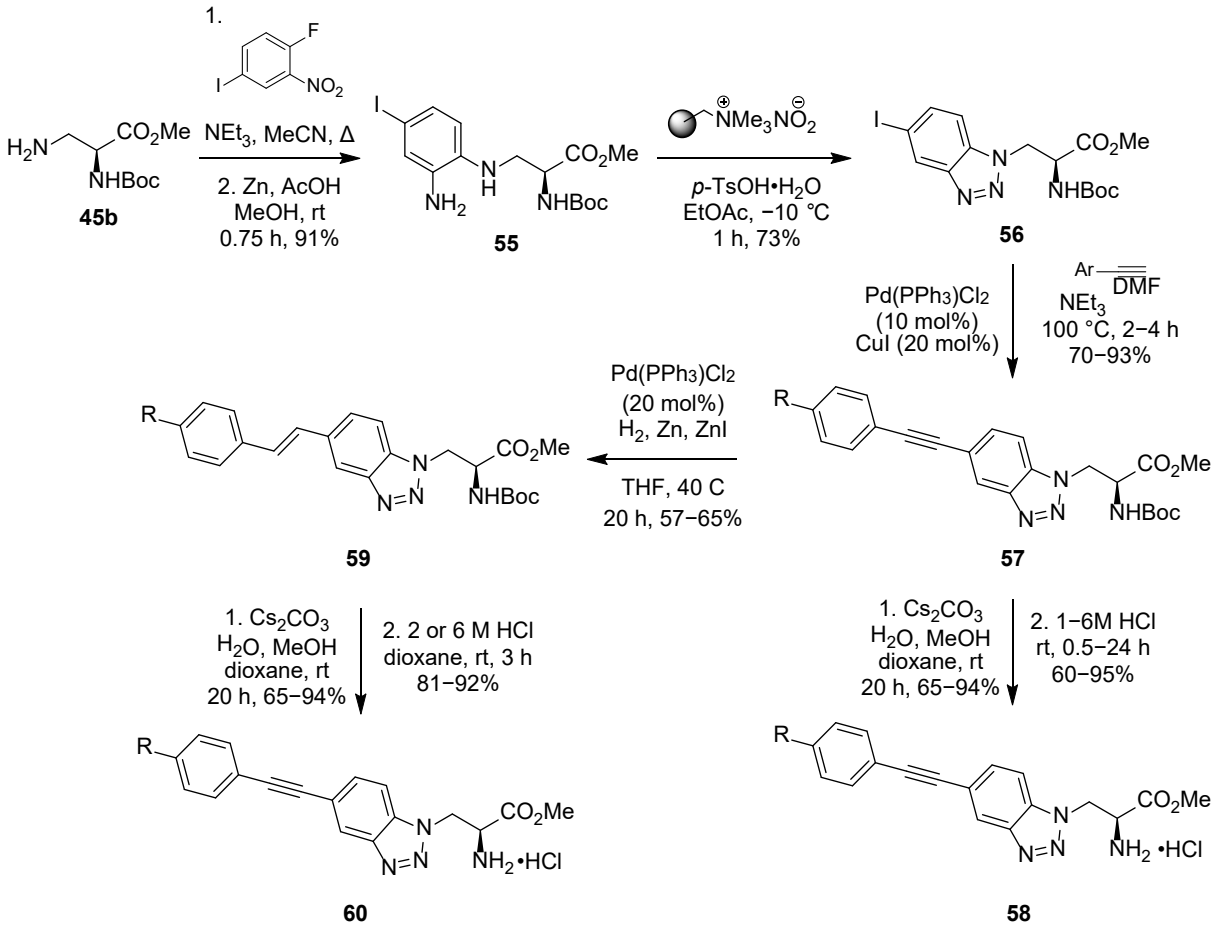

Scheme 14: Synthetic route towards conjugated benzotriazole α-amino acid derivatives with alkyne and alkene spacers

In more recent work, a novel class of thiazoloindole fluorescent α-amino acids **65** were developed (Scheme 15).[56] This structure was achieved starting from tryptophan derivative **4b** which underwent a thoiarylation at the C-2 position, with *N*-(2-bromophenylthio)succinimide and catalysed by iron(III) triflimide. The resulting compound **61** was then subject to an Ullmann-type cyclisation with copper(I) thiophene-2-carboxylate (CuTc), which gave the [3,2-α] thiazoloindole ring **62**. This core could then be further functionalised by bromination to **63** and a Suzuki-Miyaura coupling reaction to the fluorophore **64** with extended conjugation. Final deprotection gave the final hydrochloride salts **65**. It was shown that those thiazoloindole α-amino acids with electron-deficient arene substituents possessed bright charge transfer fluorescence with improved quantum yields and re-shifted absorption and emission in comparison to the tryptophan starting material. Two of these α-amino acid also

displayed compatibility with two-photon absorption by near-IR excitation, leading to potential application for biological imaging.

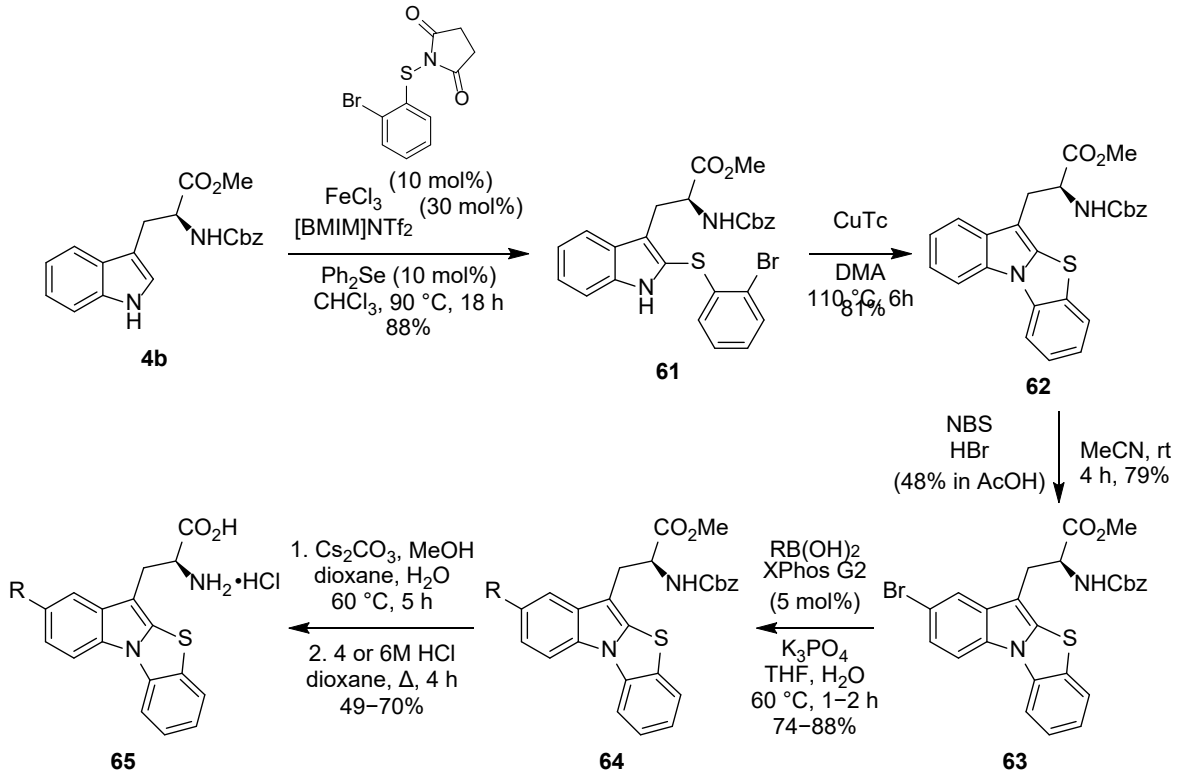

Scheme 15: Synthetic route towards thiazoloindole fluorescent α-amino acid

Most recently, the group has developed carbazole-based fluorescent α-amino acids **70** to mimic tryptophan (Scheme 16).[57] This was achieved by converting the alcohol of the Boc-protected serine derivative **66** to the iodide **67**, by mesylation and then a Finkelstein reaction. This iodide **67** was combined with zinc dust to form an organozinc intermediate. Subsequently, the reaction of the organozinc compound with a series of substituted carbazoles in Pd-catalysed Negishi couplings with SPhos as a ligand gave the carbazole α-amino acid **69**. These were deprotected in two steps to give the target compounds **70**. These compounds were then successful in mimicking tryptophan when replacing Trp residue in a beta hairpin TrpZip1 peptide. These carbazole α-amino acids also showed red-shifted absorption and emission with high quantum yields in photophysical studies. The cyano-substituted carbazole was integrated into a peptide ligand and used to measure binding to a WW domain protein.

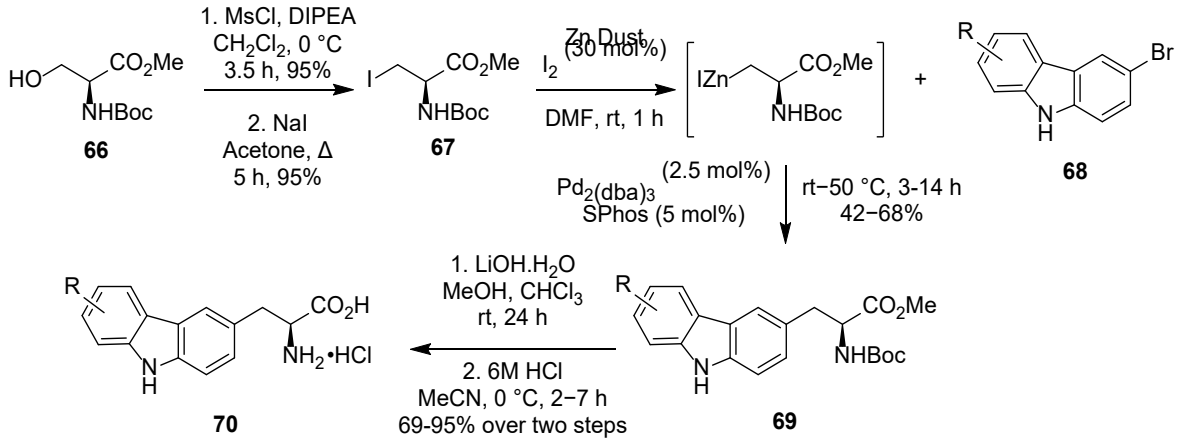

Scheme 16: Synthetic route towards carbazole-based fluorescent α-amino acid to mimic tryptophan

Charge-transfer based pyrimidine α-amino acids were also prepared in a four-step synthetic process (Scheme 17).[58] This started with the two-step conversion of an aspartic acid derivative **71** to an ynone via a Weinreb amide **72** which gave access to the ynone compounds **73** by reaction with a series of terminal alkynes. The key step then involved the creation of the pyrimidine ring in **74** using an ytterbium-catalysed heterocyclisation process of the **73** with amidines. Deprotection of the amino and ester groups gave the final fluorescent α-amino acids **75**. Determination of the photophysical properties revealed that the combination of electron-rich arene substituents with the electron deficient pyrimidine resulted in bright fluorophores with high quantum yields.

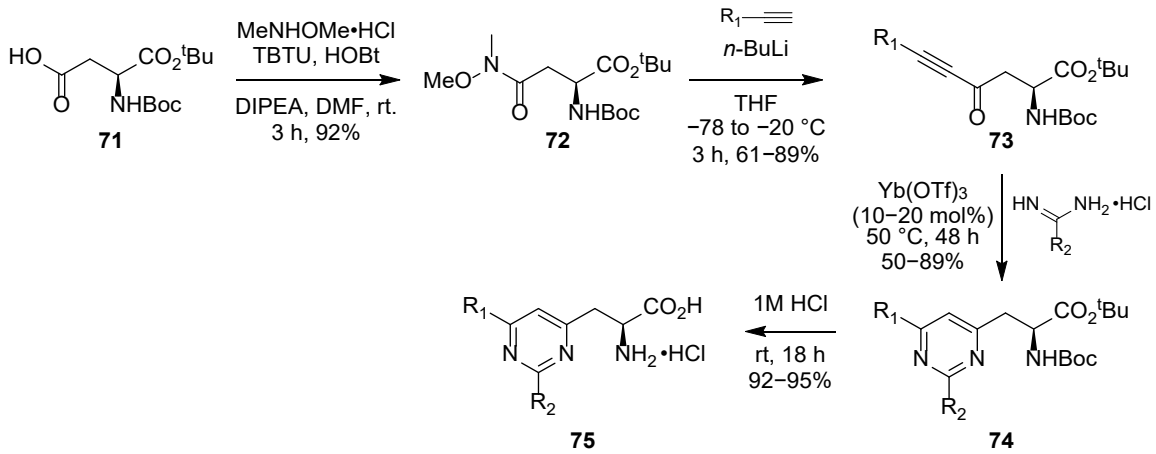

Scheme 17: Four-step synthetic route towards charge-transfer based pyrimidine α-amino acid

1.3 Aims of the Project

This project aimed to develop the synthesis of various fluorescent α-amino acids using the fluorophore design principles outlined to expand the library of available fluorophore labels for the study of biological processes.

The first class investigated will be phenoxathiin α-amino acids. This will build on previous work performed in the group and focus on extending the conjugation of the fluorophore (Scheme 18). This will involve resynthesising the phenoxathiine core **79** and then finding conditions for a regioselective bromination reaction. To extend the conjugation of the fluorophore, by the installation of an additional aromatic ring, the bromo-derivative would then be subjected to Suzuki-Miyaura reactions.

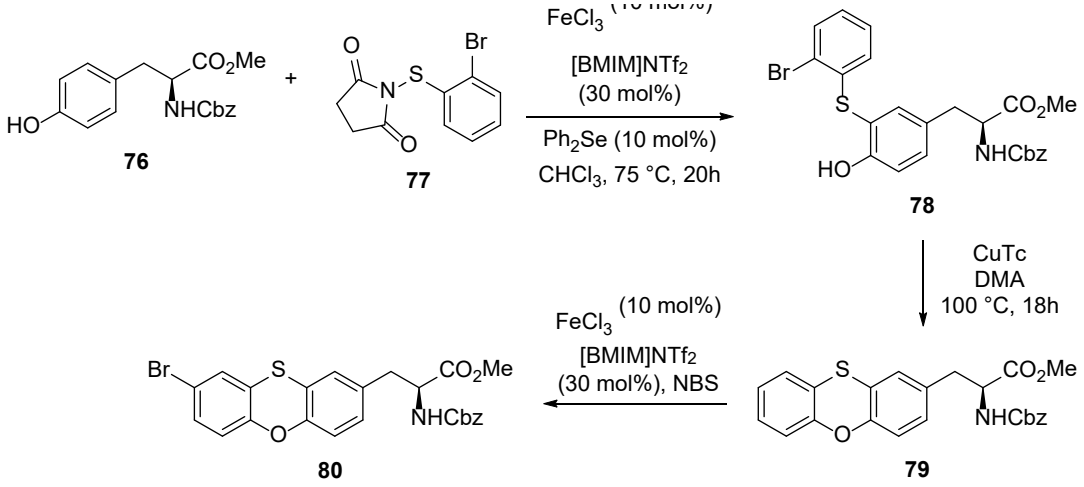

Scheme 18: Proposed synthetic route towards brominated phenoxathiin α-amino acid

The second project will focus on accessing **85**, a nitro-substituted dibenzofuran α-amino acid (Scheme 19). Previously, work in the group has utilised a key palladium-catalysed cyclisation step to form the dibenzofuran scaffold from a biaryl α-amino acid precursor with various substituents. However, these have proved to be low-yielding reactions. This project aims to access the new nitro-substituted dibenzofuran amino acid using the previous palladium-catalysed method and to compare this strategy to an alternative copper acetate mediated approach which has shown promise in cyclisations to form benzothieno[3,2-b]benzofurans.[59] This will first involve the synthesis of the cyclisation precursor **84**. This will be accomplished by Boc protection

of the L-tyrosine methyl ester **81**, bromination of the protected tyrosine derivative **82** followed by a subsequent Suzuki-Miyaura coupling reaction to form the cyclisation precursor **84**. After which the different cyclisation conditions will then be investigated for the construction of the final nitro-substituted dibenzofuran α-amino acid **85**.

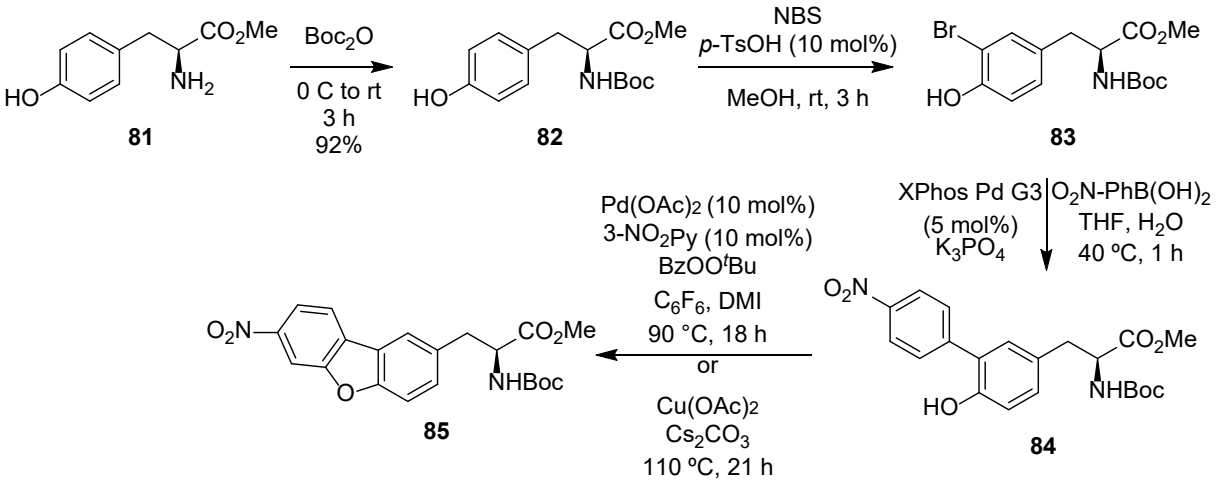

Scheme 19: Proposed modified synthetic route towards substituted dibenzofuran α-amino acid

2.0 Results and Discussion

2.1 Synthesis of Phenoxathiin Derived Amino Acid

Preparation of *N*-thiosuccinimide Reagent

Using the route previously developed in the group,[60] the synthesis of the phenoxathiin derived amino acid was carried out. This started with the synthesis of the *N*-thiosuccinimide reagent **77** (Scheme 20). To achieve this, *N*-chlorosuccinimide **87** was reacted with 2-bromothiophenol **86** using triethylamine as a base. The reaction was conducted for 6 h and after purification gave thiosuccinimide product **77**, in 74% yield.

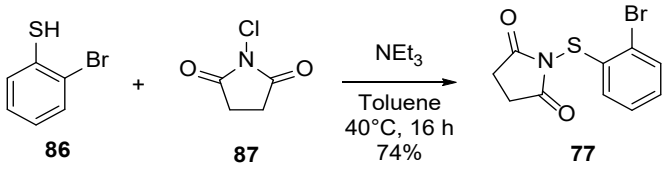

Scheme 20: Synthesis of N-(2-Bromophenylthio)succinimide

Thioarylation of Tyrosine Derivative

To conduct thioarylation of tyrosine, iron(III) triflimide was prepared from iron(III) chloride and, the ionic liquid, [BMIM]NTf_2 (Scheme 21). Iron(III) triflimide is a super Lewis acid that has been shown previously by the group to activate succinimide reagents and catalyse various arene substitution reactions.[61] Iron(III) triflimide coordinates to the Lewis basic oxygen atoms of the succinimide, which weakens the N–S bond for subsequent electrophilic aromatic substitution.

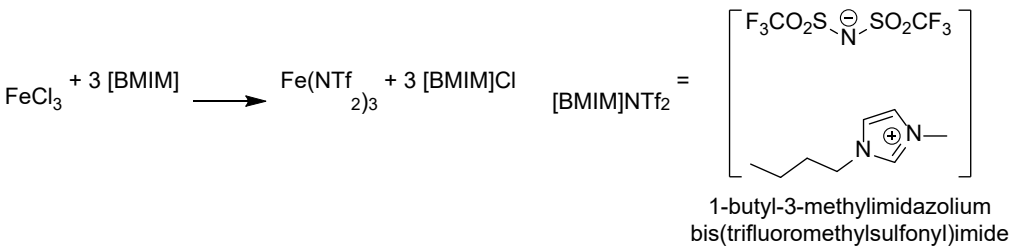

Scheme 21: In situ formation of iron(III) triflimide

Iron(III) triflimide (10 mol%) was then used to catalyse the *ortho*-thioarylation of the protected tyrosine derivative **76** with the succinimide reagent, **77** (Scheme 22). Previous work in the group showed that this reaction benefited from dual catalysis, using bis(4-methoxyphenyl)sulfane as the Lewis base. However, more recent work demonstrated that diphenyl selenide was more effective for challenging thioarylations (see mechanism below). Thus, diphenyl selenide (10 mol%) was also added to the reaction. Despite this, the reaction did not reach full conversion. After 45 h, the reaction mixture was purified to obtain thioarylated tyrosine derivative **78** in 80% yield.

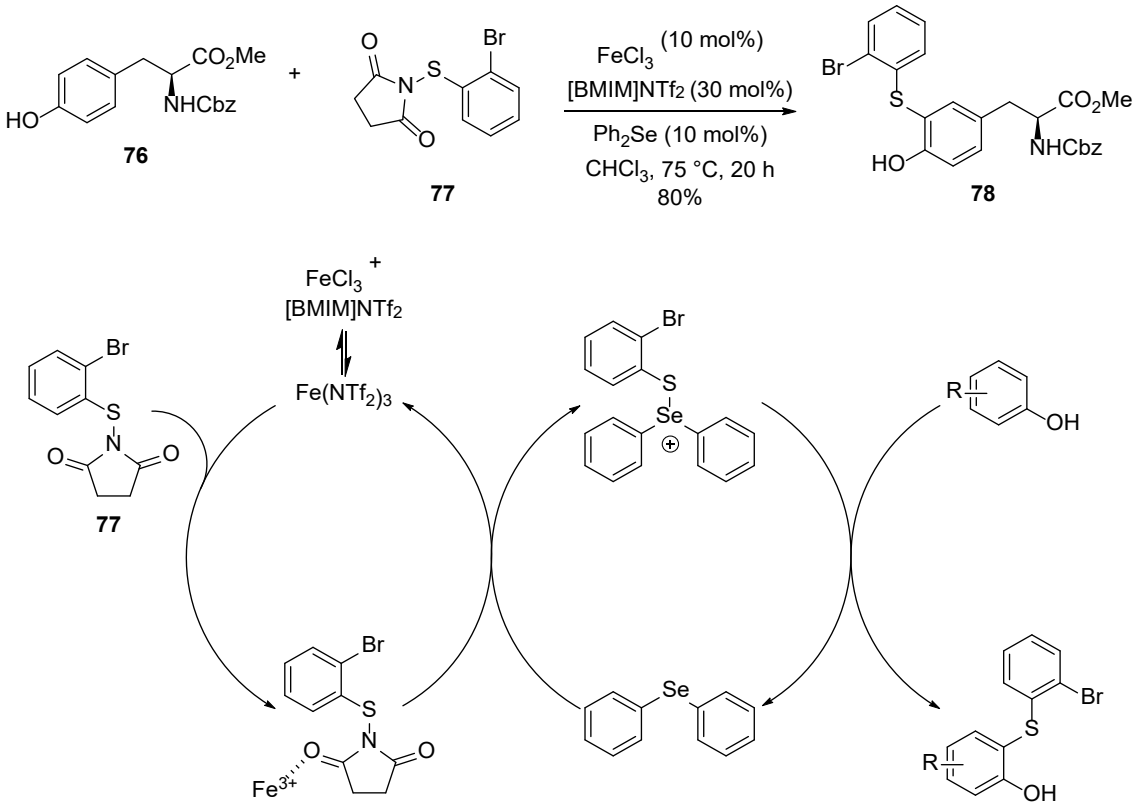

Scheme 22: Synthesis of N-(benzyloxycarbonyl)-[3'-(2''-bromophenylthio)]-L-tyrosine methyl ester and proposed mechanism of dual-catalysed iron triflimide thioarylations.

Copper-mediated cyclisation to form the phenoxathiin scaffold

Next, the Ullmann-type intramolecular cyclisation of the aryl thioether **78** was performed using stoichiometric quantities of copper(I) thiophene-2-carboxylate (CuTc) (Scheme 23). To prevent the competing intermolecular process, the reaction was

carried out at low concentration (0.03 M). After 18 h at 100 °C, the reaction gave phenoxathiin amino acid **79** in 94% yield.

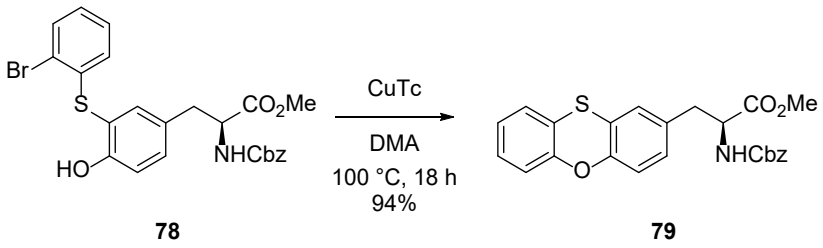

Scheme 23: Synthesis of methyl (2S)-2-[(benzyloxycarbonyl)amino]-3-(phenoxathiin-2'-yl)propanoate

Halogenation of Phenoxathiin

Having constructed the phenoxathiin structure, the next step was the bromination reaction. To achieve this, the iron(III) triflimide catalyst was utilised in conjunction with *N*-bromosuccinimide at 70 °C (Scheme 24). However, this resulted in incomplete conversion of the starting material **79**. Isolation of the product proved difficult, as product **80** and starting material **79** do not form distinct spots by TLC. The reaction was repeated at 80 °C but conversion remained incomplete. Further attempts with *N*-Iodosuccinimide were attempted with the same conditions, however, full conversion was not achieved which caused the same separation issues as with the bromination reaction.

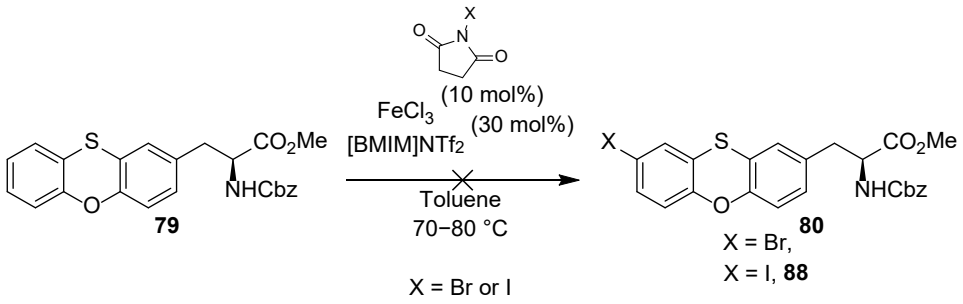

Scheme 24: Attempted halogenation of phenoxathiin amino acid with Iron(III) triflimide and succinimide reagents

As isolation of the product from the crude mixture was not achieved, harsher conditions were employed in an attempt to push the reaction to full conversion. To

attempt this, a combination of *N*-bromosuccinimide and *p*-tosic acid was used (Scheme 25). At room temperature, the reaction resulted in low consumption of starting material. To push this further, the reaction was heated to 40 °C. The higher temperature did result in some conversion to the product but caused significant degradation of the starting material.

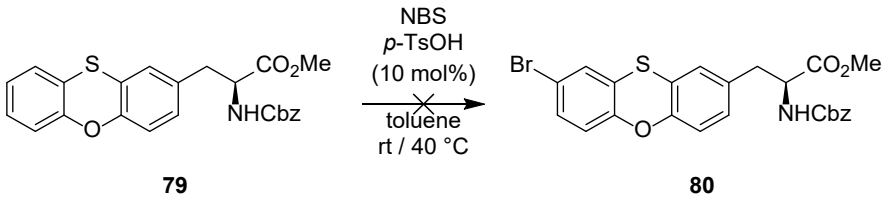

Scheme 25: Attempted bromination of phenoxathiin amino acid with NBS and p-tosic acid

An alternate approach to the attempted halogenation involved replacing the succinimide reagents with equivalent saccharin reagents. This was first attempted using *N*-chlorosaccharin which had been previously synthesised in the group (Scheme 26). The iron(III) triflimide catalyst was again utilised, now with *N*-chlorosaccharin and the phenoxathiin **79** at 70 °C in acetonitrile. After 20 hours, the reaction still showed incomplete consumption of the phenoxathiin starting material **79** but gave a conversion similar to that shown by NBS.

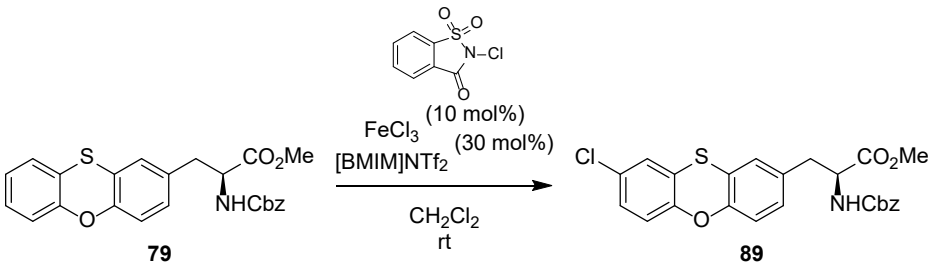

Scheme 26: Attempted chlorination of phenoxathiin with N-chlorosaccharin reagent

This led to the new approach with *N*-iodosaccharin which had the potential to provide a more reactive halogenation reaction and hopefully allow for full conversion. This synthesis of the *N*-iodosaccharin reagent **93** was achieved by following the procedure by Dolenc et al (Scheme 27).[62] This first involved combining saccharin **90**, with sodium

methoxide to generate the sodium salt. Sodium salt **91** was then reacted with silver nitrate to exchange the counterion and provide **92**, the silver salt of saccharin. Finally, iodination of **92** with iodine at room temperature and gave *N*-iodosaccharin (**93**) in 78% yield over the three steps.

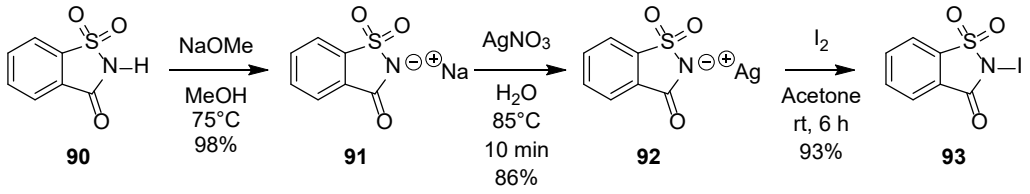

Scheme 27: Synthetic route of N-iodosaccharin starting material via sodium and silver salt intermediates

Saccharin reagent **93** was then investigated for the iodination of phenoxathiin amino acid **79** (Scheme 28). This was attempted by again generating the iron(III) triflimide catalyst in situ and then adding it to a solution of *N*-iodosaccharin (**93**) and phenoxathiin amino acid **79**. After stirring at room temperature for 17 hours, the reaction showed partial consumption of the substrate so a new reaction was attempted at 40 °C. It was found that after reaction at 40 °C for 12 hours with 2.1 equivalents of *N*-iodosaccharin (**93**) added in 3 batches (1.1 equivalents at the start of the reaction, 0.7 equivalents after 6 hours and 0.3 equivalents after 10 hours), the phenoxathiin substrate **79** was fully consumed. Unfortunately, analysis of the product proved not to be the iodinated phenoxathiin **88** that had been targeted. Full characterisation of the product showed that the reaction with the saccharin reagent had oxidised the sulfur atom to form the phenoxathiin sulfoxide α-amino acid **94**. After extensive purification, sulfoxide **94** was isolated in 12% yield. The proposed mechanism for the formation of **94** starts with iodination of the sulfur atom by reaction with **93** followed by the attack of water at the positively charged sulfur atom. Loss of a proton and then elimination of hydrogen iodide would give sulfoxide **94**.

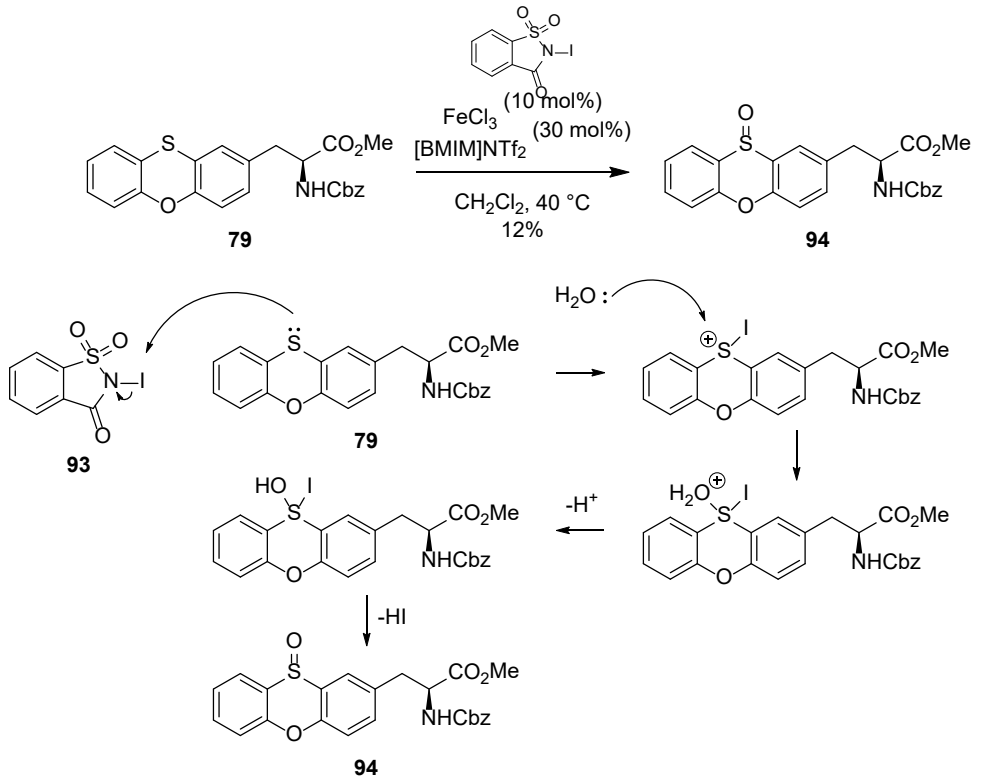

Scheme 11: Reaction scheme and proposed mechanism for the oxidation of to form the novel phenoxathiine-oxide α-amino acid

As this was a novel unnatural amino acid, absorption and emission spectra were recorded to assess its photophysical properties (Figure 9). This gave the absorption and emission wavelengths of **94** to be λ_{abs} = 226 nm and λ_{em} = 328 nm. As expected, the absorption and emission maxima wavelengths of compound **94** were, therefore, lower than that of the equivalent sulfone which had been previously synthesised in the group (λ_{abs} = 272 nm and λ_{emm} = 372 nm).

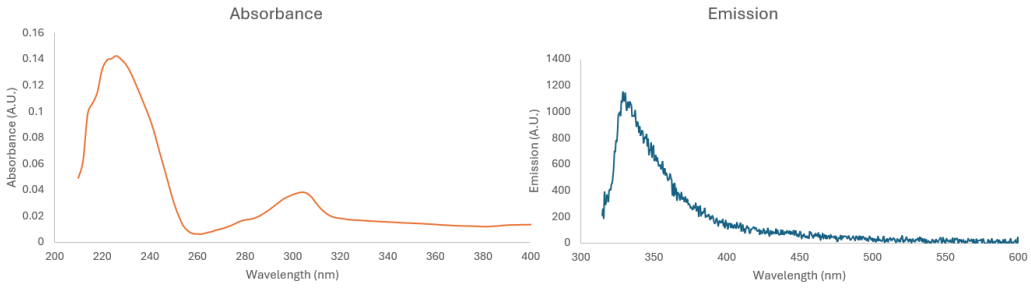

*Figure 9: Absorbance and emission spectra of compound **94** (in methanol at 10 μM)*

2.2 Synthesis of Dibenzofuran Amino Acids

Boc protection of the tyrosine derivative

The start of the synthetic route first required further protection of the methyl-ester protected tyrosine **81** by installation of a Boc-group at the amine. This was achieved by adding triethylamine and di-*tert*-butyl dicarbonate to a solution of protected tyrosine **81** using an established literature protocol (Scheme 29).[63] This gave protected α-amino acid **82** in 92% yield.

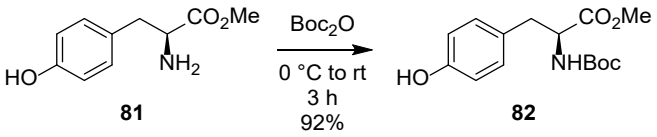

Scheme 12: Synthesis of methyl (2S)-2-(tert-butoxycarbonyl)amino-3-(4-hydroxyphenyl)propanoate

Bromination of tyrosine derivative

The next step in this synthesis was bromination of the protected tyrosine derivative **82** (Scheme 30). This was achieved by the reaction of Boc-L-tyrosine methyl ester **82** with *N*-bromosuccinimide and *p*-tosic acid (10 mol%), which gave *ortho*-bromo product **83** in 69% yield.

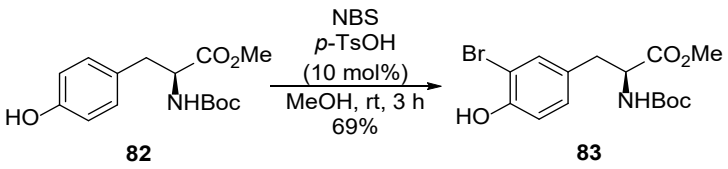

Scheme 30: Synthesis of methyl (2S)-3-(3'-bromo-4'-hydroxyphenyl)-2-[(tert-butoxycarbonyl)amino]propanoate

Suzuki-Miyaura reacton with 4-nitrobenzeneboronic acid

In the next step, the Suzuki-Miyaura coupling reaction of brominated tyrosine derivative **83** with 4-nitrobenzeneboronic acid was carried out (Scheme 31). Previous work in the group showed that phenol protection was required with other boronic acids for successful reaction, however, 4-nitrobenzeneboronic acid was shown to couple

using the unprotected phenol. The reaction was catalysed using $PdCl_2$(dppf), which has a large bite angle and is effective for sterically demanding cross-coupling reactions.[64] After 21 h at 120 °C, this gave product **84** in 88% yield. It is notable that for other substituted boronic acids this reaction required MOM protection of the phenol group, however, for the nitro-substituted compound the Suzuki reaction showed better yields with the unprotected variant **83**.

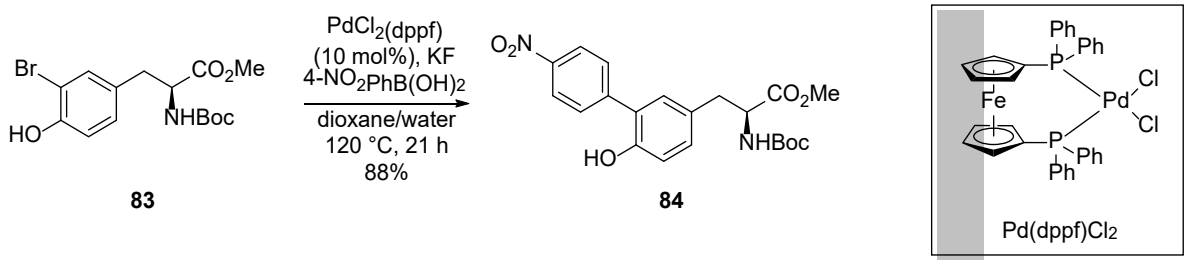

Scheme 31: Synthesis of (2S)-2-(tert-butoxycarbonyl)amino-3-[3'-(4"-nitrophenyl)-4'-hydroxyphenyl]propanoate and structure of $Pd(dppf)Cl_2$ catalyst

Palladium(II)-catalysed cyclisation to form nitro-substituted dibenzofuran

Compound **84** can now act as a precursor in the key cyclisation step to form the dibenzofuran ring system. This was attempted using a Pd-catalysed method originally developed by Wang *et al*.[65] However, this methodology was later improved upon, increasing the reaction speed, by the Wei group.[66] The conditions employed by Wei were, therefore, applied to this substrate. The cyclisation mechanism operates via an initial C–H activation at the phenolic group (Scheme 32). There is then an oxidation of the Pd(II) by *tert*-butyl peroxybenzoate (BzOO^{t}Bu) to Pd(IV). A final reductive elimination then re-generates the active catalyst and produces the dibenzofuran product.

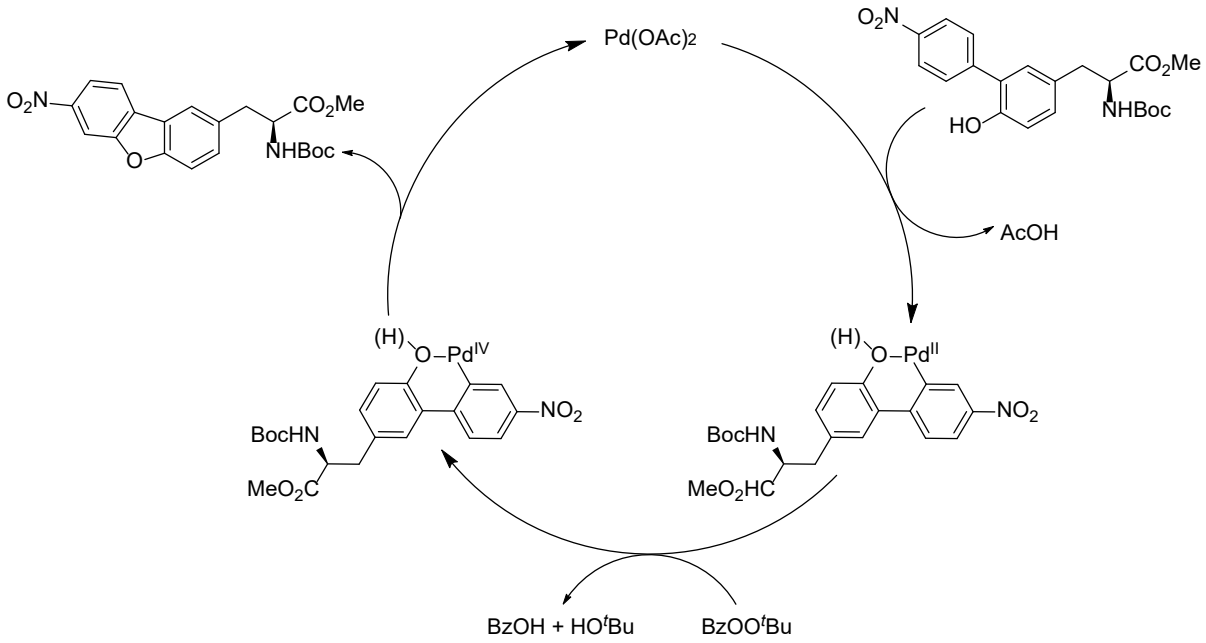

Scheme 32: Palladium(II)-catalysed cyclisation to form dibenzofuran

This method was applied to biaryl precursor **84** by reaction with palladium(II) acetate and BzOO^{t}Bu in hexafluorobenzene and 1,3-dimethyl-2-imidazolidinone (DMI) at 90 °C for 18 hours (Scheme 33). Despite the forcing conditions, this gave after column chromatography dibenzofuran product **85** in a 6% yield. As alternative conditions and higher catalyst loading failed to improve the outcome, other cyclisation methods were considered.

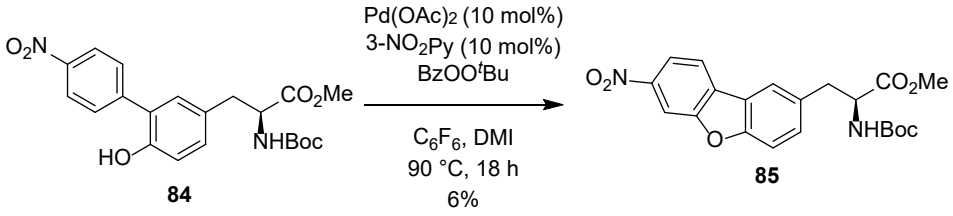

Scheme 33: Palladium(II)-catalysed cyclisation to form the nitro-substituted dibenzofuran α-amino acid

Copper(II) acetate-mediated cyclisation to form nitro-substituted dibenzofuran

Due to the low yielding palladium-catalysed C-H activation and cyclisation, an alternative metal-catalysed cyclisation method was investigated. In 2011, Li and co-workers showed that copper acetate via a radical mechanism could be used to form

furan rings as part of a larger benzothieno[3,2-b]benzofuran system.[59] This reaction was carried out with compound **84** in an attempt to improve the yield to dibenzofuran **85**, by using copper(II) acetate as a single electron transfer (SET) acceptor during the cyclisation (Scheme 27). The reaction was initially performed under argon using balloons to vent argon through the flask and degas the reaction mixture. However, this set up gave crude reaction mixtures with several side products and low conversion to the target product. Hence, the procedure was adjusted and a Young's flask and alternative approach for degassing and backfilling with argon was investigated. These modifications resulted in a much cleaner product and the target nitro-substituted dibenzofuran amino acid, **85** was isolated in an improved yield of 16%.

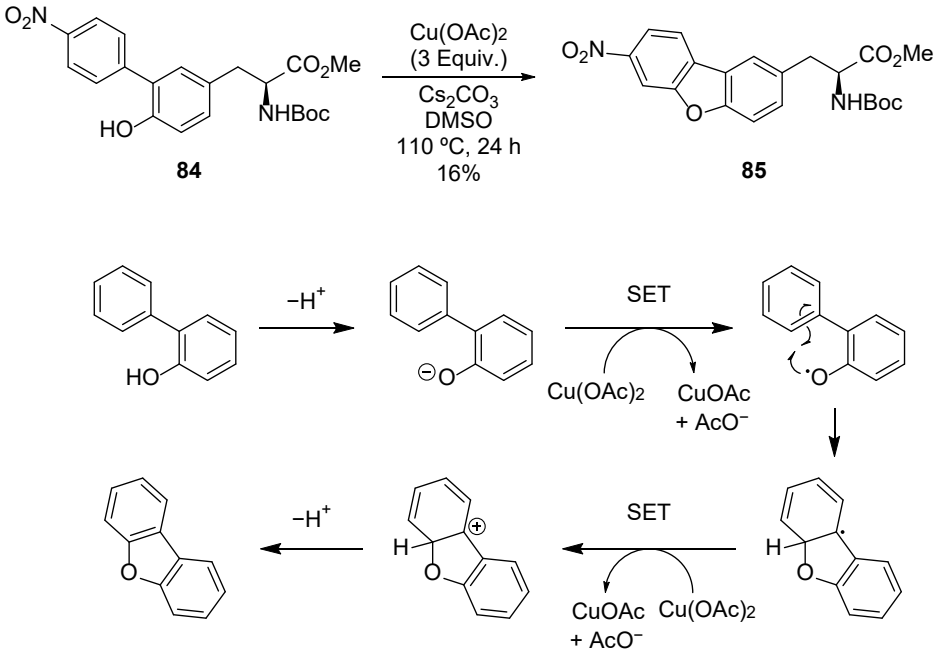

Scheme 34: Synthesis of methyl (2S)-2-(tert-butoxycarbonyl)amino-3-(7'-nitrodibenzo[b,d]furan-2'-yl)propanoate and proposed $Cu(OAc)_2$ SET mechanism

3.0 Conclusions

In conclusion, a new synthesis of phenoxathiin α-amino acid **79** was developed using a dual-catalysed Lewis acid and Lewis base approach for the key thioarylation step. In this project, diphenylselenide was found to be a highly effective Lewis base for the reaction resulting in the thioarylated product in 80% yield. Following copper-mediated cyclisation to the phenoxathiine ring, several methods were investigated for halogenation. However, the halogenated products could not be separated from the starting material and when more forcing conditions were used, this led to oxidation of the sulfur atom, resulting in isolation of a novel sulfoxide analogue. The photophysical data for this compound were recorded showing with λ_{abs} = 226 nm and λ_{em} = 328 nm.

In a second project, methods were investigated for the preparation of dibenzofuran α-amino acids. Initially, an *ortho*-arylation tyrosine substrate was successfully synthesised by regioselective bromination and a Suzuki-Miyaura cross-coupling reaction. Palladium(II)-catalysed activation and cyclisation was successful but gave the desired dibenzofuran amino acid in only 6% yield. Instead, a copper(II) acetate mediated SET process for cyclisation was investigated and gave the dibenzofuran α-amino acid in an improved 16% yield.

4.0 Future Work

Future work on the phenoxathiin amino acid project could involve developing an optimised process for the halogenation of the phenoxathiin scaffold without oxidising the sulfur atom, which will allow access through Suzuki-Miyaura reactions to further conjugation of the π-systems. Additionally, electron-withdrawing and electron-donating substituents could be implemented to give electronically interesting systems in order to improve the photophysical properties of the phenoxathiin.

For the dibenzofuran project, future work could involve further optimisation of the reaction conditions to form the cyclised dibenzofuran α-amino acid product. Once optimised conditions have been found, the next step could be to apply these reaction conditions to the various other dibenzofuran targets which were previously accessed through palladium cyclisation reactions in low yields. This would allow an optimised route to a range of substituted dibenzofurans.

5.0 Experimental

General Information

Reagents and starting materials were obtained from commercial sources and used as received. Reactions were performed open to air unless otherwise mentioned. Brine refers to a saturated aqueous solution of sodium chloride. Flash column chromatography was performed using silica gel 60 (35–70 μm). Aluminium-backed plates pre-coated with silica gel 60F_{254} were used for thin layer chromatography and were visualised with a UV lamp or by staining with Ninhydrin or Vanillin. ^{1}H NMR spectra were recorded on an NMR spectrometer at 400 MHz and data are reported as follows: chemical shift in ppm relative to tetramethylsilane (δ_H 0.00) or residual chloroform (δ_H 7.26) as the internal standard multiplicity (s = singlet, d = doublet, t = triplet, q = quartet, m = multiplet or overlap of non-equivalent resonances, integration). ^{13}C NMR spectra were recorded on an NMR spectrometer at 101 MHz and data are reported as follows: chemical shift in ppm relative to tetramethylsilane (δ_C 0.0 ppm) or residual chloroform (δ_C 77.0 ppm) as internal standard, multiplicity with respect to hydrogen (deduced from DEPT experiments, C, CH, CH_2 or CH_3). Melting points are uncorrected.

N-(2-Bromophenylthio)succinimide (77)[67]

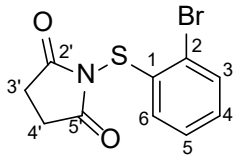

A round bottomed flask was charged with a solution of *N*-chlorosuccinimide (1.78 g, 13.3 mmol) in toluene (28 mL) under an atmosphere of argon. To the flask was added a solution of 2-bromothiophenol (1.55 mL, 12.9 mmol) in toluene (20 mL) dropwise and the resulting suspension was left to stir at 40 °C for 1 h. A solution of triethylamine (1.85 mL, 13.3 mmol) in toluene (20 mL) was added dropwise and the resulting reaction mixture was left to stir at 40 °C for 16 h. The reaction mixture was concentrated under reduced pressure and the resulting residue was dissolved in water

(30 mL). The aqueous layer was extracted with dichloromethane (3 × 30 mL). The combined organic layers were washed with brine (50 mL), dried over $MgSO_4$, filtered and concentrated *in vacuo* to yield the crude product. Purification by flash column chromatography (hexane/ethyl acetate, 3:2) gave *N*-(2-bromophenylthio)succinimide (2.74 g, 74%) as a white solid. Mp 126−129 °C (lit.[67] 128−130 °C); δ_H (400 MHz, $CDCl_3$) 2.97 (4H, s, 3'-H_2 and 4'-H_2), 6.80 (1H, dd, *J* 8.0, 1.5 Hz, 6-H), 7.06−7.11 (1H, m, 4-H), 7.22−7.27 (1H, m, 5-H), 7.52 (1H, dd, *J* 8.0, 1.3 Hz, 3-H); δ_C (101 MHz, $CDCl_3$) 29.0 (2 × CH_2), 119.2 (C), 125.2 (CH), 128.2 (CH), 128.4 (CH), 133.3 (CH), 135.5 (C), 175.9 (2 × C); *m/z* (ESI) 310 (MNa^+. 100%).

_N_-(Benzyloxycarbonyl)-[3'-(2''-bromophenylthio)]-L-tyrosine methyl ester (78)[60]

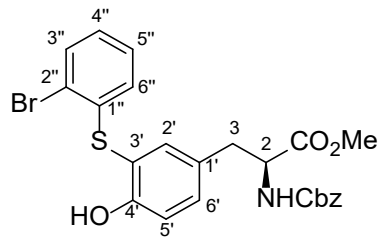

Iron(III) trichloride (11.8 mg, 0.0730 mmol, 10 mol%) was dissolved in [BMIM]NTf_2 (64.0 µL, 0.220 mmol, 30 mol%) and left to stir for 0.5 h at room temperature before being added to a solution of *N*-(2-bromophenylthio)succinimide (250 mg, 0.873 mmol) in chloroform (1.5 mL). *N*-(Benzyloxycarbonyl)-L-tyrosine methyl ester (241 mg, 0.733 mmol) was then added and the reaction mixture was left to stir at 75 °C for 45 h. The reaction mixture was concentrated *in vacuo.* Purification by flash column chromatography (dichloromethane) gave *N*-(benzyloxycarbonyl)-[3'-(2''-bromophenylthio)]-L-tyrosine methyl ester (303 mg, 80%) as a colourless oil. $[\alpha]_D^{25}$ +42.7 (*c* 0.1, $CHCl_3$); δ_H (400 MHz, CDCl3) 3.01 (1H, dd, *J* 14.0, 5.8 Hz, 3-*H*H), 3.11 (1H, dd, *J* 14.0, 5.5 Hz, 3-H*H*), 3.67 (3H, s, CO_2CH_3), 4.63 (1H, ddd, *J* 8.0, 5.8, 5.5 Hz, 2-H), 5.07 (1H, d, *J* 12.2 Hz, PhC*H*H), 5.10 (1H, d, *J* 12.2 Hz, PhCH*H*), 5.29 (1H, d, *J* 8.0 Hz, NH), 6.36 (1H, s, OH), 6.53 (1H, dd, *J* 8.0, 1.5 Hz, 6''-H), 6.95–7.03 (2H, m, 5'- H and 4''-H), 7.05–7.12 (1H, m, 5''-H), 7.15 (1H, dd, *J* 8.4, 2.2 Hz, 6'-H), 7.28–

7.39 (6H, m, 2'-H and Ph), 7.52 (1H, dd, *J* 7.9, 1.3 Hz, 3''-H); δ_C (101 MHz, $CDCl_3$) 37.4 (CH_2), 52.6 (CH_3), 55.0 (CH), 67.2 (CH_2), 115.4 (C), 116.2 (CH), 121.1 (C), 126.8 209 (CH), 127.1 (CH), 128.2 (2 × CH), 128.3 (CH), 128.4 (CH), 128.7 (2 × CH), 129.2 (C), 133.1 (CH), 133.9 (CH), 136.3 (C), 137.3 (C), 137.9 (CH) 155.6 (C), 156.8 (C), 171.8 (C); *m/z* (ESI) 538.0288 (MNa^+. $C_{24}H_{22}{}^{79}BrNNaO_5S$ requires 538.0294).

Methyl (2*S*)-2-[(benzyloxycarbonyl)amino]-3-(phenoxathiin-2'-yl)propanoate (79)[60]

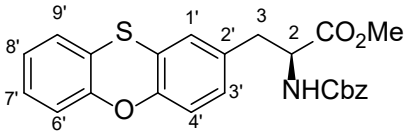

To a solution of *N*-(benzyloxycarbonyl)-[3'-(2''-bromophenylthio)]-L-tyrosine methyl ester (250 mg, 0.483 mmol) in *N,N*-dimethylacetamide (16.1 mL) was added copper(I) thiophene-2-carboxylate (92.3 mg, 0.484 mmol). The reaction mixture was stirred at 100 °C for 18 h. The reaction mixture was extracted with ethyl acetate (30 mL) and washed with 5% aqueous lithium chloride (3 × 30 mL). The aqueous layer was further extracted with ethyl acetate (2 × 20 mL). The organic layers were combined and further washed with 5% aqueous lithium chloride (3 × 20 mL), dried over $MgSO_4$, filtered and concentrated *in vacuo*. Purification by flash column chromatography (dichloromethane) gave methyl (2*S*)-2-[(benzyloxycarbonyl)amino]-3-(phenoxathiin-2'-yl)propanoate (97.8 mg, 94%) as a colourless oil. $[\alpha]_D^{25}$ +48.7 (*c* 0.1, $CHCl_3$); δ_H (400 MHz, $CDCl_3$) 2.98 (1H, dd, *J* 14.0, 6.0 Hz, 3-*H*H), 3.06 (1H, dd, *J* 14.0, 5.6 Hz, 3-H*H*), 3.73 (3H, s, CO_2CH_3), 4.62 (1H, ddd, *J* 8.0, 6.0, 5.6 Hz, 2-H), 5.08 (1H, d, *J* 12.2 Hz, PhC*H*H), 5.13 (1H, d, *J* 12.2 Hz, PhCH*H*), 5.23 (1H, d, *J* 8.0 Hz, NH), 6.81–6.85 (2H, m, 1'-H and 4'-H), 6.87–6.91 (1H, m, 3'-H), 6.97–7.02 (2H, m, 6'-H and 8'-H), 7.08 (1H, dd, *J* 7.7, 1.5 Hz, 9'-H), 7.10–7.14 (1H, m, 7'-H), 7.29–7.38 (5H, m, Ph); δ_C (101 MHz, $CDCl_3$) 37.5 (CH_2), 52.6 (CH_3), 54.9 (CH), 67.2 (CH_2), 117.9 (CH), 118.0 (CH), 119.9 (C), 120.5 (C), 124.7 (CH), 126.9 (CH), 127.5 (CH), 127.9 (CH), 128.2 (2 × CH), 128.4 (CH), 128.7 (CH), 128.7 (2 × CH), 132.3 (C), 136.3 (C), 151.4 (C), 152.2 (C), 155.7 (C) 171.9 (C); *m/z* (ESI) 458.1031 (MNa^+. $C_{24}H_{21}NNaO_5S$ requires 458.1033).

_N_-Iodosaccharin (93)[62]

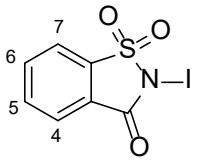

To a solution of saccharin (0.500 g, 2.73 mmol) in methanol (20 mL) was added sodium methoxide (0.148 g, 2.75 mmol). The resultant mixture was stirred at 75 °C for 1 h and the reaction mixture was then concentrated in *vacuo* to give the sodium saccharin salt (0.550 g, 2.68 mmol) as a white solid. The sodium saccharin salt was then added dropwise to a stirred solution of silver nitrate (0.451 g, 2.65 mmol) in water (3.3 mL) at 85 °C. After 10 minutes, the reaction mixture was cooled to room temperature and the precipitated silver saccharin salt was filtered, washed with water (2 × 3 mL) and acetone (2 × 1.5 mL) then left to air dry overnight with exclusion of light. The dry silver saccharin salt (0.664 g, 2.29 mmol) was then dissolved in acetone (6.5 mL) and iodine (0.613 g, 2.41 mmol) was added portionwise. The reaction flask was covered in foil to exclude light and the reaction mixture was stirred at room temperature for 6 h. Precipitated silver iodide was filtered and the filtrate was concentrated under vacuum to give *N*-iodosaccharin as a white solid (0.664 g, 78%). Spectroscopic data was in accordance with the literature.[62] δ_H (400 MHz, DMSO-d_6) 7.84–8.02 (3H, m, 4-H, 5-H and 6-H), 8.15 (1H, d, *J* 7.4 Hz, 7-H).

Methyl (2*S*)-2-[(benzyloxycarbonyl)amino]-3-(phenoxathiine-10'-oxide-2'-yl)propanoate (94)

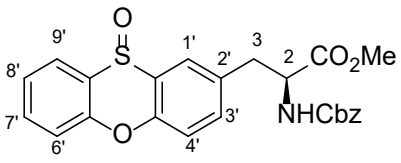

Iron(III) trichloride (1.86 mg, 0.0114 mmol) was dissolved in [BMIM]NTf_2 (10.0 µL, 34.4 µmol) and left to stir for 0.5 h at room temperature before being added to a suspension of *N*-iodosaccharin (39.9 mg, 0.129 mmol, 1.1 equiv.) in dichloromethane (0.6 mL). To the suspension was added methyl (2*S*)-2-[(benzyloxycarbonyl)amino]-3-

(phenoxathiin-2'-yl)propanoate (50.0 mg, 0.115 mmol, 1 equiv.) and the resulting reaction material was left to stir at 40 °C for 6 h. A second batch of *N*-iodosaccharin (23.9 mg, 77.3 μmol, 0.67 equiv.) was then added to the reaction vessel which was left to stir further at 40 °C for 4 h. A third batch of *N*-iodosaccharin (11.9 mg, 38.5 μmol, 0.33 equiv.) was added and the reaction mixture was stirred for a final 2 h at 40 °C. The reaction mixture was cooled to room temperature and concentrated *in vacuo*. The resulting residue was diluted with ethyl acetate (20 mL) and washed with 1 M aqueous sodium thiosulfate (20 mL). The aqueous layer was further extracted with ethyl acetate (3 × 20 mL). The combined organic layers were dried over $MgSO_4$, filtered and concentrated *in vacuo*. Purification by flash chromatography (dichloromethane/methanol) gave methyl (2*S*)-2-[(benzyloxycarbonyl)amino]-3-(phenoxathiine-10'-oxide-2'-yl)propanoate as a colourless oil (6.30 mg, 12%). $[\alpha]_D^{19}$ – 17.9 (*c* 0.1, MeOH); ν_{max}/cm^{-1} (neat) (NH), 3293 (NH), 3059, 2922 (CH) 1716, (C=O), 1212; δ_H (400 MHz, $CDCl_3$) 3.06–3.32 (2H, m, 3-H_2), 3.75 (3H, s, CO_2CH_3), 4.69 (1H, dq, *J* 12.9, 6.7 Hz, 2-H), 5.04–5.13 (2H, m, $PhCH_2$), 5.32 (1H, d, *J* 6.7 Hz, NH), 7.27–7.46 (9H, m, 3'-H, 4'-H, 6'-H, 8'-H and Ph), 7.58–7.71 (2H, m, 1'-H and 7'-H), 7.92 (1H, dd, *J* 7.8, 1.8 Hz, 9'-H); δ_C (101 MHz, $CDCl_3$) 37.6 (CH_2), 52.7 (CH), 54.7 (CH_3), 67.2 (CH_2), 118.8 (CH), 118.9 (CH), 119.0 (CH), 123.5 (C), 123.7 (C), 124.9 (CH), 128.2 (2 × CH), 128.3 (CH), 128.6 (2 × CH), 131.1 (CH), 131.4 (CH), 131.5 (CH), 132.9 (C), 133.0 (C),133.8 (CH), 134.6 (CH), 134.8 (CH), 136.1 (C),148.5 (C), 149.4 (C), 155.5 (C); *m/z* (ESI) 452 (MH^+. 100%).

Methyl (2*S*)-2-[(*tert*-butoxycarbonyl)amino]-3-(4-hydroxyphenyl)propanoate (82)[66]

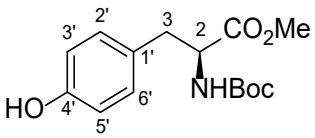

To a round bottomed flask was added methyl (2*S*)-2-amino-3-(4-hydroxyphenyl)propanoate hydrochloride (1.00 g, 4.32 mmol) and methanol (5 mL). The solution was cooled to 0 °C before the addition of triethylamine (1.80 mL, 13.0 mmol) and di-*tert*-butyl dicarbonate (1.09 mL, 4.75 mmol). The reaction mixture was stirred for 15 minutes at 0 °C and then for 3 h at ambient temperature. The solvent

was removed under reduced pressure, and the crude material was purified by silica gel column chromatography (eluent system 1:1 hexane:ethyl acetate) to give methyl (2*S*)-2-[(*tert*-butoxycarbonyl)amino]-3-(4-hydroxyphenyl)propanoate as a white solid (1.17 g, 92%). R_f = 0.47 (1:1 hexane:ethyl acetate); Mp 99–100 °C (lit.[66] 100–102 °C); $[\alpha]_D^{23}$ +46.0 (*c* 1.0, $CHCl_3$); δ_H (500 MHz, $CDCl_3$) 1.40 (9H, s, 3 × CH_3), 2.94 (1H, dd, *J* 14.0, 5.9 Hz, 3-*H*H), 3.00 (1H, dd, *J* 14.0, 5.9 Hz, 3-H*H*), 3.67 (3H, s, OMe), 4.54–4.48 (1H, m, 2-H), 5.13 (1H, d, *J* 8.2 Hz, NH), 6.73 (2H, d, *J* 8.3 Hz, 2'-H), 6.93 (2H, d, *J* 8.3 Hz, 3'-H); δ_C (126 MHz, $CDCl_3$) 28.4 (3 × CH_3), 37.6 (CH_2), 52.4 (CH_3), 54.8 (CH), 80.4 (C), 115.7 (2 × CH), 127.4 (C), 130.4 (2 × CH), 155.4 (C), 155.5 (C), 172.8 (C); *m/z* (ESI) 318 (MNa^+. 100%).

Methyl (2*S*)-3-(3'-bromo-4'-hydroxyphenyl)-2-[(*tert*-butoxycarbonyl)amino]propanoate (83)[68]

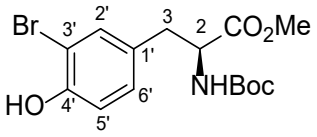

To a stirred solution of methyl (2*S*)-2-[(*tert*-butoxycarbonyl)amino]-3-(4'-hydroxyphenyl)propanoate (247 mg, 0.836 mmol) and *p*-toluenesulfonic acid (16.2 mg, 0.0851 mmol, 10 mol%) in methanol (0.8 mL) in a foiled round bottomed flask was added a solution of *N*-bromosuccinimide (151 mg, 0.848 mmol) in methanol (8.7 mL) dropwise from a foiled dropping funnel over 0.2 h. The reaction mixture was stirred at room temperature for 3 h. The reaction mixture was concentrated *in vacuo*. Purification by flash column chromatography (dichloromethane/ethyl acetate, 20:1) gave methyl (2*S*)-2-[(*tert*-butoxycarbonyl)amino]-3-(3'-bromo-4'-hydroxyphenyl)propanoate (218 mg, 69%) as a white solid. Mp 111–115 °C (lit.[68] 117–119 °C); $[\alpha]_D^{21}$ +45.7 (*c* 0.1, $CHCl_3$); δ_H (400 MHz, $CDCl_3$) 1.43 (9H, s, O*t*Bu), 2.95 (1H, dd, *J* 14.0, 5.9 Hz, 3-H), 3.05 (1H, dd, *J* 14.0, 5.2 Hz, 3-H), 3.72 (3H, s, CO_2Me), 4.47–4.57 (1H, m, 2-H), 4.98 (1H, d, *J* 8.2 Hz, NH), 5.43 (1H, s, OH), 6.90–7.03 (2H, m, 5'-H and 6'-H), 7.23 (1H, d, *J* 1.5 Hz, 2'-H); δ_C (101 MHz, $CDCl_3$) 28.4 (3 × CH_3), 37.4 (CH_2), 52.5 (CH_3), 54.6

(CH), 80.3 (C), 110.3 (C), 116.2 (CH), 129.9 (C), 130.2 (CH), 132.8 (CH), 151.5 (C), 155.2 (C), 172.3 (C); *m/z* (ESI) 396 (MNa^+. 100%).

Methyl (2*S*)-2-[(*tert*-butoxycarbonyl)amino]-3-[3'-(4''-nitrophenyl)-4'-hydroxyphenyl]propanoate (84)

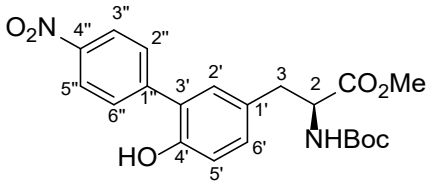

A solution of methyl (2*S*)-3-(3'-bromo-4'-hydroxyphenyl)-2-[(*tert*-butoxycarbonyl)amino]propanoate (299 mg, 0.800 mmol), 4-nitrophenylboronic acid (270 mg, 1.62 mmol), potassium fluoride (141 mg, 2.42 mmol) and $PdCl_2$(dppf) (59.1 mg, 0.0808 mmol, 10 mol%) in dioxane (6.5 mL) and water (1.0 mL) was degassed under argon for 0.3 h. The reaction mixture was stirred at 120 °C for 21 h. The reaction mixture was then diluted in ethyl acetate (20 mL) and washed in 0.5 M hydrochloric acid (3 × 20 mL) and brine (3 × 20 mL). The organic layer was then dried ($MgSO_4$), filtered and concentrated. Purification by column chromatography (hexane/ethyl acetate, 4:1 gradient) gave methyl (2*S*)-2-[(*tert*-butoxycarbonyl)amino]-3-[3'-(4''-nitrophenyl)-4'-hydroxyphenyl]propanoate (294 mg, 88%) as a yellow solid. Mp: 55–56 °C; $[\alpha]_D^{17}$ +44.2 (*c* 0.1, $CHCl_3$); ν_{max}/cm^{-1} (neat) 3372 (NH), 2978 (CH), 1682 (C=O), 1657 (C=O), 1508, 1435, 1396, 1342; δ_H (500 MHz, $CDCl_3$) 1.40 (9H, s, O^{t}Bu), 2.98 (1H, dd, *J* 13.9, 6.0 Hz, 3-*H*H), 3.10 (1H, dd, *J* 13.9, 6.0 Hz, 3-H*H*), 3.72 (3H, s, CO_2Me), 4.60–4.54 (1H, m, 2-H), 5.13 (1H, d, *J* 8.3 Hz, NH), 6.70 (1H, s, OH), 6.80 (1H, d, *J* 8.2 Hz, 5'-H), 6.99 (1H, d, *J* 8.2 Hz, 6'-H), 7.03 (1H, d, *J* 1.9 Hz, 2'-H), 7.68 (2H, d, *J* 8.3 Hz, 2''-H and 6''-H), 8.21 (2H, d, *J* 8.3 Hz, 3''-H and 5''-H); δ_C (126 MHz, $CDCl_3$) 28.4 (3 × CH_3), 37.7 (CH_2), 52.6 (CH_3), 54.7 (CH), 80.6 (C), 116.8 (CH), 123.6 (2 × CH), 126.2 (C), 128.4 (C), 130.1 (2 × CH), 130.9 (CH), 131.5 (CH), 145.0 (C), 146.8 (C), 152.4 (C), 155.4 (C), 172.6 (C); *m/z* (ESI) 439.1472 (MNa^+. $C_{21}H_{24}NNaO_7$ requires 439.1476).

Methyl (2*S*)-2-[(*tert*-butoxycarbonyl)amino]-3-(7'-nitrodibenzo[b,d]furan-2'-yl)propanoate (85)

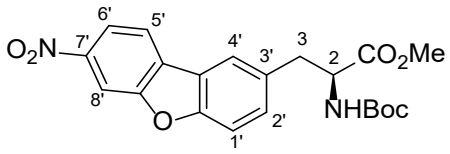

Methyl (2*S*)-2-[(*tert*-butoxycarbonyl)amino]-3-[3'-(4''-nitrophenyl)-4'-hydroxyphenyl]propanoate (49.5 mg, 0.119 mmol), caesium carbonate (39.6 mg, 0.122 mmol) and copper acetate (66.2 mg, 0.364 mmol) were added to an oven-dried Young's flask. The flask was then evacuated and refilled with argon four times. Anhydrous DMSO (2.4 mL) was then added under positive pressure of argon and the flask was sealed. The reaction mixture was then heated to 110 °C and left to stir for 18 h. The flask was allowed to cool to room temperature before the solution was acidified with 1 M hydrochloric acid (12 mL). This was then extracted with dichloromethane (4 × 10 mL) and the combined organic layers were washed with water (4 × 10 mL). The organic layer was then dried with $MgSO_4$, filtered and concentrated *in vacuo*. Purification by column chromatography (hexane/ethyl acetate, 4:1) gave methyl (2*S*)-2-[(*tert*-butoxycarbonyl)amino]-3-(7'-nitrodibenzo[b,d]furan-2'-yl)propanoate (8.00 mg, 16%) as a yellow oil. $[\alpha]_D^{17}$ +40.7 (*c* 0.1, $CHCl_3$); ν_{max}/cm^{-1} (neat) 3354 (NH), 2926 (CH), 2356, 2341, 1691 (C=O), 1519, 1472, 1340, 2157, 822; δ_H (400 MHz, $CDCl_3$) 1.40 (9H, s, O^{t}Bu), 3.16–3.37 (2H, m, 3-H_2), 3.74 (3H, s, CO_2Me), 4.66 (1H, q, *J* 6.6 Hz, 2-H), 5.06 (1H, d, *J* 8.2 Hz, NH), 7.36 (1H, dd, *J* 8.4, 1.6 Hz, 2'-H), 7.58 (1H, d, *J* 8.4 Hz, 1'-H), 7.81 (1H, d, *J* 1.6 Hz, 4'-H), 8.02 (1H, d, *J* 8.8 Hz, 5''-H), 8.28 (1H, dd, *J* 8.4, 2.0 Hz, 6'-H), 8.44 (1H, d, *J* 2.0 Hz, 8'-H); δ_C (101 MHz, $CDCl_3$) 28.3 (3 × CH_3), 38.4 (CH_2), 52.4 (CH_3), 54.7 (CH), 80.0 (C), 108.1 (CH), 112.3 (CH), 118.5 (CH), 120.5 (CH), 122.3 (CH), 122.8 (C), 130.0 (C), 130.8 (CH), 132.1 (2 × C), 146.8 (C), 155.4 (C), 157.5 (C), 172.2 (C); *m/z* (ESI) 315.0976 ([M+H]-Boc$^+$. $C_{16}H_{14}N_2O_5$ requires 315.0975).

6.0 References

1 D. M. Jameson, Introduction to Fluorescence, CRC Press, Boca Raton, 2014.

2 S. Benson, F. de Moliner, W. Tipping and M. Vendrell, *Angew. Chem. Int. Ed.*, 2022, **61**, e2022047.

3 Z. Cheng, E. Kuru, A. Sachdeva and M. Vendrell, *Nat. Rev. Chem.*, 2020, **4**, 275–290.

4 R. Helm, A. B. Cubitt and R. Y. Tsien, *Nature*, 1995, **373**, 663–664.

5 R. Y. Tsien, *Annu. Rev. Biochem.*, 1998, **67**, 509-544.

6 C. Zhao, A. Fernandez, N. Avlonitis, G. Vande Velde, M. Bradley, N. D. Read and M. Vendrell*, ACS Comb. Sci.*, 2016, **18**, 689–696.

7 J. R. Lakowicz, Principles of fluorescence spectroscopy, Springer, Berlin, 2006.

8 T. C. Lovell, B. P. Branchaud and R. Jasti, European *J. Org. Chem.*, 2024, **24**, e202301196.

9 A. Jablonski, *Nature*, 1933, **131**, 839–840.

10 Y. Fu and N. S. Finney, *RSC Adv.*, 2018, **8**, 29051–29061.

11 A. M. Thooft, K. Cassaidy and B. Vanveller, *J. Org. Chem.*, 2017, **82**, 8842–8847.

12 J. H. Xie, Z. Y. Xu, C. C. Deng, N. B. Li and H. Q. Luo, *Sens. Actuators B Chem.*, 2023, **393**, 8134.

13 F. Bureš, *RSC Adv.*, 2014, **4**, 58826–58851.

14 H. Niu, J. Liu, H. M. O'Connor, T. Gunnlaugsson, T. D. James and H. Zhang, *Chem. Soc. Rev.*, 2023, **52**, 2322–2357.

15 Y. Urano, M. Kamiya, K. Kanda, T. Ueno, K. Hirose and T. Nagano, *J. Am. Chem. Soc.*, 2005, **127**, 4888–4894.

16 T. R. Xu, R. J. Ward, J. D. Pediani and G. Milligan, *J. Biol. Chem.*, 2012, **287**, 14937–14949.

17 B. T. Bajar, E. S. Wang, S. Zhang, M. Z. Lin, J. Chu, N. Hildebrandt, I. Medintz and R. Algar, *Sensors*, 2016, **16**, 1488.

18 J. V Jun, D. M. Chenoweth and E. J. Petersson, *Org. Biomol. Chem.*, 2020, **18**, 5747–5763.

19 A. H. Harkiss and A. Sutherland, *Org. Biomol. Chem.*, 2016, **14**, 8911–8921.

20 J. O. Escobedo, O. Rusin, S. Lim and R. M. Strongin, *Curr. Opin. Chem. Biol.*, 2010, **14**, 64–70.

21 S. Wang, B. Li and F. Zhang, *ACS Cent. Sci.*, 2020, **6**, 1302–1316.

22 J. B. Grimm and L. D. Lavis, *Nat. Methods*, 2022, **19**, 149–158.

23 Y. Yang, F. Gao, Y. Wang, H. Li, J. Zhang, Z. Sun and Y. Jiang, *Molecules*, 2022, **27**, 8421.

24 C. Sánchez-Rico, L. Voith von Voithenberg, L. Warner, D. C. Lamb and M. Sattler, *Chem. Eur. J.*, 2017, **23**,14267 –14277.

25 J. Roncali, Macromol. *Rapid Commun.*, 2007, **28**, 1761–1775.

26 X. Liu, Z. Xu and J. M. Cole, *J. Phys. Chem. C*, 2013, **117**, 16584–16595.

27 M. Dai, Y. J. Yang, S. Sarkar and K. H. Ahn, *Chem. Soc. Rev.*, 2023, **52**, 6344–6358.

28 J. Clayden, N. Greeves and S. Warren, Organic Chemistry, Oxford University Press, London, 2012.

29 J. B. Grimm, B. P. English, J. Chen, J. P. Slaughter, Z. Zhang, A. Revyakin, R. Patel, J. J. Macklin, D. Normanno, R. H. Singer, T. Lionnet and L. D. Lavis, *Nat. Methods*, 2015, **12**, 244–250.

30 L. D. Lavis and R. T. Raines, *ACS Chem. Biol.*, 2008, **3**, 142–155.

31 A. B. T. Ghisaidoobe and S. J. Chung, *Int. J. Mol. Sci.*, 2014, **15**, 22518–22538.

32 S. Lepthien, M. G. Hoesl, L. Merkel and N. Budisa, *Proc. Natl. Acad. Sci. U.S.A.*, 2008, **105**, 16905–16100.

33 M. R. Hilaire, D. Mukherjee, T. Troxler and F. Gai, *Chem. Phys. Lett.*, 2017, **685**, 133–138.

34 M. You, H. Fan, Y. Wang and W. Zhang, *Chem. Phys.*, 2019, **526**, 110438.

35 R. J. Micikas, I. A. Ahmed, A. Acharyya, A. B. Smith and F. Gai, *Phys. Chem. Chem. Phys.*, 2021, **23**, 6433–6437.

36 L. Mendive-Tapia, C. Zhao, A. R. Akram, S. Preciado, F. Albericio, M. Lee, A. Serrels, N. Kielland, N. D. Read, R. Lavilla and M. Vendrell, *Nat. Commun.*, 2016, **7**, 10940.

37 N. D. Barth, R. Subiros-Funosas, L. Mendive-Tapia, R. Duffin, M. A. Shields, J. A. Cartwright, S. T. Henriques, J. Sot, F. M. Goñi, R. Lavilla, J. A. Marwick, S. Vermeren, A. G. Rossi, M. Egeblad, I. Dransfield and M. Vendrell, *Nat. Commun.*, 2020, **11**, 4027.

38 C. D. Navo, A. Asín, E. Gómez-Orte, M. I. Gutiérrez-Jiménez, I. Compañón, B. Ezcurra, A. Avenoza, J. H. Busto, F. Corzana, M. M. Zurbano, G. Jiménez-Osés, J. Cabello and J. M. Peregrina, *Chem. Eur. J.*, 2018, **24**, 7991–8000.

39 S. Chen, N. E. Fahmi, C. Bhattacharya, L. Wang, Y. Jin, S. J. Benkovic and S. M. Hecht, *Biochemistry*, 2013, **52**, 8580–8589.

40 S. Chen, N. E. Fahmi, L. Wang, C. Bhattacharya, S. J. Benkovic and S. M. Hecht, *J. Am. Chem. Soc.*, 2013, **135**, 12924–12927.

41 L. C. Speight, A. K. Muthusamy, J. M. Goldberg, J. B. Warner, R. F. Wissner, T. S. Willi, B. F. Woodman, R. A. Mehl and E. J. Petersson, *J. Am. Chem. Soc.*, 2013, **135**, 18806–18814.

42 A. Szymańska, K. Wegner and L. Łankiewicz, *Helv. Chim. Acta*, 2003, **86**, 3326–3331.

43 G. Pereira, H. Vilaça and P. M. T. Ferreira, *Amino Acids*, 2013, **44**, 335–344.

44 C. Li, J. Tang and J. Xie, *Tetrahedron*, 2009, **65**, 7935–7941.

45 C. Li, E. Henry, N. K. Mani, J. Tang, J. C. Brochon, E. Deprez and J. Xie, *Eur. J. Org. Chem.*, 2010, 2395–2405.

46 Y. Bin Ruan, Y. Yu, C. Li, N. Bogliotti, J. Tang and J. Xie, *Tetrahedron*, 2013, **69**, 4603–4608.

47 C. Hoppmann, U. Alexiev, E. Irran and K. Rück-Braun, *Tetrahedron Lett.*, 2013, **54**, 4585–4587.

48 L. Shukla, L. W. K. Moodie, T. Kindahl and C. Hedberg, *J. Org. Chem.*, 2018, **83**, 4792–4799.

49 M. Stawikowski and G. B. Fields, *Curr. Protoc. Protein Sci.*, 2012, **69**, 18.1.1-13.

50 L. S. Fowler, D. Ellis and A. Sutherland, *Org. Biomol. Chem.*, 2009, **7**, 4309–4316.

51 A. H. Harkiss, J. D. Bell, A. Knuhtsen, A. G. Jamieson and A. Sutherland, *J. Org. Chem.*, 2019, **84**, 2879–2890.

52 J. D. Bell, A. H. Harkiss, D. Nobis, E. Malcolm, A. Knuhtsen, C. R. Wellaway, A. G. Jamieson, S. W. Magennis and A. Sutherland, *Chem. Comm.*, 2020, **56**, 1887–1890.

53 J. D. Bell, T. E. F. Morgan, N. Buijs, A. H. Harkiss, C. R. Wellaway and A. Sutherland, *J. Org. Chem.*, 2019, **84**, 10436–10448.

54 R. McGrory, D. C. Morgan, A. G. Jamieson and A. Sutherland, *Org. Lett.*, 2023, **25**, 5844–5849.

55 L. M. Riley, T. N. Mclay and A. Sutherland, *J. Org. Chem.*, 2023, **88**, 2453–2463.

56 A. C. Dodds, H. G. Sansom, S. W. Magennis and A. Sutherland, *Org. Lett.*, 2023, **25**, 8942–8946.

57 R. Clarke, L. Zeng, B. C. Atkinson, M. Kadodwala, A. R. Thomson and A. Sutherland, *Chem. Sci.*, 2024, **15**, 5944-5949.

58 S. Songsri, A. H. Harkiss and A. Sutherland, *J. Org. Chem.*, 2023, **88**, 13214–13224.

59 L. Ai, I. Y. Ajibola and B. Li, *RSC Adv.*, 2021, **11**, 36305–36309.

60 A. C. Dodds and A. Sutherland, *Org. Biomol. Chem.*, 2022, **20**, 1738–1748.

61 A. C. Dodds and A. Sutherland, *J. Org. Chem.*, 2021, **86**, 5922–5932.

62 D. Dolenc, *Synlett*., 2000, **4**, 544–546

63 P. Chen et al., *J. Med. Chem*. 1996, **39**, 1991-2007.

64 P. W. N. M. Van Leeuwen, P. C. J. Kamer, J. N. H. Reek and P. Dierkes, *Chem. Rev.*, 2000, **100**, 2741–2769.

65 X. Wang, Y. Lu, H. X. Dai and J. Q. Yu, *J. Am. Chem. Soc.,* 2010, **132**, 12203–12205.

66 Y. Wei and N. Yoshikai, *Org. Lett.,* 2011, **13**, 5504–5507.

67 W. C. Gao, T. Liu, B. Zhang, X. Li, W. L. Wei, Q. Liu, J. Tian and H. H. Chang, *J. Org. Chem.*, 2016, **81**, 11297–11304.

68 A. G. Brown, M. J. Crimmin and P. D. Edwards, *J. Chem. Soc.*, *Perkin Trans.1*, 1992, 123-130.